

1 **Myogenesis modelled by human pluripotent stem cells uncovers**
2 **Duchenne muscular dystrophy phenotypes prior to skeletal muscle**
3 **commitment**

4 Virginie Mournetas^{1*}, Emmanuelle Massouridès², Jean-Baptiste Dupont¹, Etienne Kornobis⁴, Hélène Polvèche²,
5 Margot Jarrige², Maxime Gosselin⁵; Spiros D. Garbis⁶; Dariusz C. Górecki⁵; Christian Pinset³

6 * Correspondence: vmournetas@istem.fr

7 ¹INSERM UEVE UMR861, I-STEM, AFM, 28 rue Henri Desbruères, 91100 Corbeil-Essonnes, France

8 ²CECS, I-STEM, AFM, 28 rue Henri Desbruères, 91100 Corbeil-Essonnes, France

9 ³CNRS, I-STEM, AFM, 28 rue Henri Desbruères, 91100 Corbeil-Essonnes, France

10 ⁴Institut Pasteur, 25-28 Rue du Dr Roux, 75015 Paris, France

11 ⁵Molecular Medicine, School of Pharmacy and Biomedical Sciences, University of Portsmouth, PO1 2DT,
12 Portsmouth, UK

13 ⁶Proteome Exploration Laboratory, Beckman Institute, California Institute of Technology, Division of Biology
14 and Biological Engineering, 1200 E. California Blvd., MC 139-74, Pasadena, California, 91125, USA

15 **ABSTRACT**

16 Duchenne muscular dystrophy (DMD) causes severe disability of children and death of young men, with an
17 incidence of approximately 1/5,000 male births. Symptoms appear in early childhood, with a diagnosis made
18 around 4 years old, a time where the amount of muscle damage is already significant, preventing early
19 therapeutic interventions that could be more efficient at halting disease progression. In the meantime, the
20 precise moment at which disease phenotypes arise – even asymptotically – is still unknown. Thus, there is a
21 critical need to better define DMD onset as well as its first manifestations, which could help identify early
22 disease biomarkers and novel therapeutic targets.

23 In this study, we have used human induced pluripotent stem cells (hiPSCs) from DMD patients to model
24 skeletal myogenesis, and compared their differentiation dynamics to healthy control cells by a comprehensive
25 multi-omics analysis. Transcriptome and miRnome comparisons combined with protein analyses at 7 time
26 points demonstrate that hiPSC differentiation 1) mimics described DMD phenotypes at the differentiation
27 endpoint; and 2) homogeneously and robustly recapitulates key developmental steps - mesoderm, somite,
28 skeletal muscle - which offers the possibility to explore dystrophin functions and find earlier disease
29 biomarkers.

30 Starting at the somite stage, mitochondrial gene dysregulations escalate during differentiation. We also
31 describe fibrosis as an intrinsic feature of skeletal muscle cells that starts early during myogenesis. In sum, our
32 data strongly argue for an early developmental manifestation of DMD whose onset is triggered before the
33 entry into the skeletal muscle compartment, data leading to a necessary reconsideration of dystrophin
34 functions during muscle development.

35 INTRODUCTION

36 Duchenne muscular dystrophy (DMD) is a rare genetic disease, but it is the most common form of myopathy
37 affecting approximately one in 5,000 male births and very rarely female. In this recessive X-linked monogenic
38 disorder, mutations in the DMD gene lead to the loss of a functional dystrophin protein, resulting in a
39 progressive - yet severe - muscle wasting phenotype (1). In patients, symptoms usually appear in early
40 childhood (2-5 years old) and worsen with age, imposing the use of wheelchair before 15 and leading to
41 premature death by cardiac and/or respiratory failure(s) mostly around 30 years of age (2).

42 At the age of diagnosis, around 4 years old, muscles of DMD patients have already suffered from the pathology
43 (3,4). Several reviews pointed out the limitations of current disease biomarkers, which fail to detect the
44 development of DMD specifically and at an early age (5,6). Meanwhile, no treatment is available to stop this
45 degenerative disease yet. Developing therapies aim at restoring the expression of dystrophin in muscle cells
46 but, so far, the level stays too low to be beneficial to patients (7). The absence of both reliable biomarkers and
47 effective therapies stress the need of better defining the first steps of DMD in Human to be able to 1) find
48 specific markers of disease initiation in order to increase diagnosis sensitivity and, therefore, improve patient
49 management by accelerating their access to better healthcare; and 2) develop alternative therapeutic
50 approaches by finding targets that compensate the lack of dystrophin and complement current attempts at
51 restoring its expression (8).

52 In 2007, a seminal publication reported that the gene expression profile of muscles from asymptomatic DMD
53 children younger than 2 years old is already distinguishable from healthy muscles, suggesting that DMD
54 molecular dysregulations appear before disease symptomatic manifestations (4). Evidence obtained in
55 multiple animal models, such as neonatal *GRMD* dogs (9), DMD zebrafish (10) and *mdx* mouse embryos (11), as
56 well as in human fetuses (12–14) even suggest that DMD starts before birth, during prenatal development.
57 Our team recently identified the embryonic dystrophin isoform Dp412e expressed in early mesoderm-
58 committed cells (15), another indication that DMD can start *in utero*. Further exploring DMD onset in human
59 fetuses is extremely challenging for obvious ethical and practical reasons. A way to overcome these issues is
60 to develop a human DMD model *in vitro*, recapitulating embryonic development from human pluripotent stem
61 cells to skeletal muscle lineages.

62 To our knowledge, none of the existing human DMD *in vitro* models, either based on tissue-derived myoblasts
63 (16) or on the differentiation of induced pluripotent stem cells (17–21), have been used for studying DMD
64 during the ontogeny of the skeletal muscle lineage. Moreover, original protocols for *in vitro* myogenesis from
65 human pluripotent stem cells (reviewed in (22)) use transgene overexpression or/and cell sorting procedures,
66 and thereby, miss the steps preceding skeletal muscle commitment, *e.g.* paraxial mesoderm and myotome.
67 Novel protocols have recently used transgene-free directed differentiation to recapitulate human embryonic
68 development in a dish, giving theoretical access to the developmental steps (19,23–25).

69 In the present study, we compared the myogenic differentiation dynamics of healthy and DMD hiPSCs using a
70 multi-omic approach to identify early disease manifestations *in vitro*. DMD cells showed marked transcriptome
71 dysregulations from day 10, before the detection of skeletal muscle regulatory factors at day 17. Specifically,
72 we identified the dysregulation of mitochondrial genes as one of the earliest detectable phenotypes. These
73 alterations escalated over the course of muscle specification. In addition, we showed an early induction of
74 Sonic hedgehog signalling pathway, followed by collagens as well as fibrosis-related genes suggesting the
75 existence of an intrinsic fibrotic process solely driven by DMD muscle cells. Overall, our data highlight that
76 human pluripotent stem cells are a suitable cell model to study muscle development in both healthy and
77 disease conditions. In the context of DMD, they strongly argue for the existence of early disease
78 manifestations during somite development.

79 RESULTS

80 To establish the early/developmental impact of *DMD* gene mutations, human induced pluripotent stem cells
81 (hiPSCs) from three DMD patients and three healthy individuals were generated as described previously (15).
82 These cells, when subjected to a standardised differentiation protocol without utilisation of feeder cells, cell
83 sorting or gene overexpression, formed elongated and plurinucleated myotubes within 25 days (23), with an
84 amplification fold of 2918 ± 480 (mean \pm SEM). Skeletal muscle progenitor cells after 17 days of differentiation
85 could be cryopreserved (Figure S1A). Whole transcriptome and miRnome profiles were compared at 7
86 differentiation time points (tissue-derived myoblasts and myotubes, as well as hiPSC-derived cells at days 0, 3,
87 10, 17 and 25) and complemented by iTRAQ proteomics and Western blot analyses (Table S1).

88 DMD is initiated prior to the expression of skeletal muscle markers

89 First, the expression profile of the *DMD* variants was studied by RT-qPCR in healthy and DMD hiPSCs during the
90 differentiation process described in Figure S1A. The *Dp427m* variant, which is normally observed in muscle
91 cells (26), appeared from day 17, in contrast with *Dp412e* – the embryonic variant of dystrophin present in
92 mesoderm cells (15) – which was expressed at differentiation day 3. Therefore, the expression of the *DMD*
93 locus is initiated in the very first steps of our differentiation protocol, well before myotube formation. The
94 ubiquitous variant *Dp40-71* was detected at every time points, in contrast with *Dp116* (Schwann cell variant
95 (27)), *Dp140* (kidney and foetal brain variant (28)) and *Dp427p1p2* (Purkinje cell variant (29)), which were all
96 undetected at the examined time points (Figure S1B). Interestingly, *Dp260* (retinal variant (30)) followed a
97 similar expression pattern than *Dp427m*. *Dp427c* (cerebral variant (31)) was also detected at days 17 and 25,
98 but at a very low level. As expected, DMD cells expressed lower levels of *Dp427m* and *Dp260* (Figure S1B).

99 A strong correlation in the transcriptomic data was observed by mRNA-seq and miRNA-seq between samples
100 collected at an individual time point, as opposed to samples from two distinct time points. In addition, the
101 correlation coefficient between samples taken at two successive time points increased as differentiation
102 progressed (Figure 1A). Differential expression analysis between two successive collection days (days 3/0, days
103 10/3, days 17/10, days 25/17) in healthy controls showed that the proportion of regulated genes decreased
104 from 20 % to 12 % of the whole transcriptome (2223 to 1284 mRNAs, adjusted pvalue ≤ 0.01) through the
105 course of differentiation. These observations demonstrate the robustness of the differentiation protocol and
106 are in agreement with an early specialisation and a later refinement of the transcriptome as cells quickly exit
107 pluripotency and become progressively restricted to the skeletal muscle lineage.

108 To characterise the developmental stages achieved by the cells, the expression of lineage-specific markers
109 (both mRNAs and miRNAs) was determined at each time point, together with gene enrichment analyses
110 (Figure 1B-2A, Figure S2B-C, Table S2).

111 Pluripotency was similarly maintained in healthy and DMD cells at day 0 (Figure 2A – Table S2), as already
112 shown by our group (15). At day 3, cells lost pluripotency and became paraxial mesoderm cells expressing
113 marker genes such as *PAX3* and *PAX7* (11) (Figure 2A, Table S2). Importantly, markers of lateral plate (*GATA4*
114 (32) and *NKX2-5* (33)) and intermediate mesoderm (*PAX8* (34) and *ORS1* (35)) were undetected at this stage
115 (Table S2). Similarly, earlier markers of primitive streak (*EOMES* (36) and *TBX6* (37)), mesendoderm (*NODAL*
116 (38) and *MIXL1* (39)), as well as markers of the other germ layers endoderm (*AFP* (40) and *SOX17* (41)) and
117 ectoderm (*PAX6* (42) and *SOX2* (43)) were either not expressed or greatly downregulated (Table S2),
118 suggesting cell homogeneity in the differentiation process.

119 At that early time point, DMD-associated gene dysregulation represented less than 3 % of the entire
120 transcriptome (adjusted pvalue ≤ 0.05 , Figure 2B) but already contained genes important for development
121 (e.g. *MEIS2* (44)) and muscle formation (e.g. *ACTA1* (45)). However, mesoderm markers were not significantly
122 dysregulated, attesting that mesoderm commitment was mostly unimpaired (Figure 2A – Table S2). No

123 increase in the expression of primitive streak, mesendoderm, endoderm or ectoderm markers was detected,
124 suggesting no differences in the differentiation process of DMD cells at that stage (Table S2).

125 In contrast, a sharp increase in the proportion of dysregulated genes appeared at day 10 compared to day 0
126 and day 3, mostly including gene downregulations (DMD/Healthy expression ratio ≤ 0.76 , adjusted pvalue \leq
127 0.05). This concerned almost 10 % of the transcriptome at day 10 (against 3 % at day 3) and remained stable
128 from 10 to 12 % (1226 mRNAs) until day 25 (Figure 2B). At day 10, healthy cells started to express genes
129 typically observed during somitogenesis, such as *PAX3* (46) *NR2F2* (47), *PTN* (48), *MET* (49), *H19* and *IGF2* (50)
130 (Table S2). More precisely, their transcriptome exhibits a mixed profile between dermomyotome (expression
131 of *GLI3* (51) and *GAS1* (52) but not *ZIC3* (53)) and myotome (expression of *MET* (54) and *EPHA4* (55) but not
132 *LBX1* (56)) (Table S2). Neither markers of presomitic mesoderm cells (*MSGN1* (57) and *FGF8* (58)) and neural
133 plate cells (*SIX1* (59) and *FOXD3* (60)), nor markers of sclerotome (*PAX1* (61) and *PAX9* (62)) and dermatome
134 (*EGFL6* (63)) were expressed (Table S2). In DMD cells, no increase of presomitic mesoderm, neural plate,
135 sclerotome or dermatome markers was observed (Table S2). In the meantime, several somite markers were
136 downregulated, including *H19*, *IGF2*, *MET* and *SEMA6A* (64) (validated at the protein level for SEMA6A, Figure
137 2A-S3A – Table S2), while a slight upregulation of dermomyotome and chondrocyte markers was highlighted
138 and confirmed at the protein level for GLI3 (Figure S3B), together with a significant enrichment of the gene
139 ontology term ‘neurogenesis’, suggesting potential lineage bifurcations at day 10 (Figure 2A-S2C – Table S2).

140 The study of differentiation dynamics presented above highlights that mesoderm commitment is not impaired
141 by the absence of dystrophin, and shows that DMD onset takes place at the somite cell stage, before the
142 expression of the skeletal muscle program and especially before the expression of *Dp427m*, the muscle variant
143 of the *DMD* gene.

144 **DMD hiPSC can become skeletal muscle progenitor cells, but exhibit specific muscle gene dysregulations**

145 Healthy and DMD cells were in the skeletal muscle compartment at day 17, as evidenced by the expression of
146 multiple lineage-specific genes and proteins, such as transcription factors (e.g. *MYOD1* (65)), cell surface
147 markers (e.g. *CDH15* (66)), sarcomere genes (e.g. *TNNC2* (67)), dystrophin-associated protein complex (DAPC)
148 genes (e.g. *SGCA* (68)), Calcium homeostasis genes (e.g. *RYR1* (69)) and muscle-specific miRNAs (myomiR, e.g.
149 *miR-1* (70)), (Figure 1B, Table S2). They both showed an embryonic/foetal phenotype characterised by *ERBB3*
150 expression, in contrast with tissue-derived myoblasts that expressed *NGFR* (21). Here again, alternative cell
151 lineages were absent or greatly downregulated, such as tenocytes (*MKX* (71) and *SCX* (72)), chondrocytes
152 (*SOX5* and *SOX9* (73)), osteoblasts (*SP7* (74) and *SPP1* (75)) or nephron progenitors (*SIX2* (76) and *SALL1* (77))
153 (Table S2).

154 Interestingly, DMD cells did not show dysregulated expression of skeletal muscle transcription factors (Table
155 S2). However, several myomiRs were found downregulated (e.g. *miR-1*, Figure 2C), together with genes related
156 to calcium homeostasis (e.g. *ATP2A2* (78), at both mRNA and protein level, Figure 2D-E) as well as members of
157 the DAPC (e.g. *SNTA1* (79)) (Table S2). Concerning cell lineages, there was no visible difference when
158 compared to healthy controls, except an upregulation of markers associated with chondrocytes, which was
159 confirmed at the protein level for GLI3 (Figure S3C), and a significant enrichment of the gene ontology term
160 ‘neurogenesis’ previously seen at day 10 (Figure 2A-S2C – Table S2).

161 Therefore, DMD cells efficiently enter the skeletal muscle compartment at day 17, but exhibit dysregulations in
162 several features typically associated with dystrophic muscles, which could be a direct consequence of the early
163 manifestations of DMD detected at day 10.

164 **hiPSC differentiation lead to embryonic/foetal myotubes that reproduce DMD phenotypes**

165 As previously described (23), both healthy and DMD hiPSC-derived myotubes (day 25) were able to twitch
166 spontaneously in culture, and fluorescent staining of nuclei and α -actinin confirmed cell fusion and the
167 formation of striation patterns typical of muscle fibres *in vivo* (Figure 3A). Western blot analyses on protein

168 extracts from DMD cells confirmed that dystrophin was either undetectable or slightly expressed (Figure 3B),
169 as in the corresponding patient muscle biopsies.

170 We selected representative mRNAs and miRNAs and showed that both hiPSC-derived and tissue-derived
171 myotubes have exited the cell cycle and upregulated genes expressed in skeletal muscles (Figure S4A, Figure
172 4A, Table S2). This included skeletal muscle myomiRs (miR-1, miR-133 and miR-206 (80,81)), transcription
173 factors involved in skeletal myogenesis including those of the MRF family (e.g. *MYOD1* (65), *MYOG* (82)),
174 specific muscle cell surface markers (e.g. *CDH15* (66), *ITGA7* (83)) as well as genes involved in the formation of
175 the DAPC (e.g. *SGCA* (68), *DTNA* (84)), sarcomeres (e.g. *TNNC2* (67), *TNNT3* (85)), myofibril organisation (e.g.
176 *UNC45B* (86), *NACA* (87)) and the execution of excitation-contraction coupling at the neuromuscular junction
177 (NMJ, e.g. *MUSK* (88), *DOK7* (89)) (Figure 4A, Table S2).

178 Even though global analysis showed that hiPSC-derived myotubes were similar to their tissue-derived
179 counterparts in term of lineage commitment, they displayed an embryonic/foetal phenotype – as suggested in
180 progenitors at day 17. This can be illustrated by the expression of the embryonic/foetal myosin heavy/light
181 chains *MYH3* (90), *MYH8*(91), *MYL4* (92) and *MYL5* (93) but not the postnatal transcripts *MYH1* and *MYH2* (94),
182 which were detected in tissue-derived myotubes. Myotubes derived from hiPSCs had also higher levels of *IGF2*,
183 which is downregulated at birth (95), and expressed *DLK1*, which is known to be extinct in adult muscles (96)
184 (Figure S4B).

185 Despite the embryonic/foetal phenotype, hiPSC-derived myotubes showed evidence of terminal
186 differentiation and cellular maturation. First, their total level of myosin heavy chain proteins was significantly
187 higher than in tissue-derived myotubes, as confirmed by Western blotting (Figure 3B). RNAs and proteins
188 involved in DAPC formation (e.g. *DMD*, *SGCA* (68) and *SGCG* (97)), as well as in excitation-contraction coupling
189 (e.g. *RYR1* (69) and *CACNA1S* / *CAV1.1* (98)) were also present at higher levels (Figure 3B-4A). Finally, higher
190 expression of skeletal muscle transcription factors (e.g. *MEF2C* (99)), and of multiple genes involved in muscle
191 contraction (e.g. *TNNT3* (85)), NMJ formation (e.g. *RAPSN* (100)), and creatine metabolism (e.g. *CKM* (101))
192 indicates that hiPSC-derived cells expressed features of fully differentiated muscle cells (Figure 4A). Similar to
193 previous time points, day 25 cells were negative for markers of alternative muscle lineages, i.e. cardiac (*miR-*
194 *208a* (102), *MYL7* (103) and *RYR2* (104)) and smooth muscle cells (*MYH11* (105), *CNN1* (106) and
195 *CHRNA3/B2/B4* (107)).

196 In DMD cells, there was a global trend toward downregulation of muscle transcription factors, which was only
197 significant for *MEF2A* and *MEF2D* in hiPSC-derived myotubes and *EYA4* and *MYOD1* in tissue-derived myotubes
198 (Figure S4C). In addition, myomiRs previously associated with muscle dystrophy (dystromiRs, e.g. miR-1 (70),
199 Figure 2C) were found downregulated (Table S2). Similarly, a global downregulation phenotype was observed
200 in both tissue- and hiPSC-derived DMD myotubes, and concerned multiple genes associated with known
201 disease phenotypes, such as cell surface markers (e.g. *ITGA7* (83)), DAPC organisation (e.g. *SGCA* (68)),
202 myofibril organisation (e.g. *UNC45B* (86)), sarcomere formation (e.g. *MYO18B* (108)), NMJ function (e.g.
203 *CHRNA1* (109)) and calcium homeostasis (e.g. *ATP2A2* (78), Figure 2D)(Figure 4B-S2C).

204 Altogether, these data indicate that hiPSC-derived myotubes recapitulate a full skeletal muscle differentiation
205 program, and exhibit an embryonic/foetal phenotype. Importantly, it shows that disease phenotypes usually
206 observed in young adult animal models are detectable at least at the transcriptional level in human DMD
207 myotubes that display an otherwise embryonic/foetal profile. This validates the quality of this cell system to
208 model the DMD pathology.

209 **Fibrosis, an intrinsic feature of DMD cells independent of TGF- β pathway**

210 As presented above, the upregulation of chondrocyte markers in DMD cells, although already present at day
211 10, became significant from day 17 (Figure 2A – Table S2). It was accompanied by the upregulations of the
212 Sonic hedgehog (SHH) signalling pathway and of multiple collagens (Figure 5A, Table S2). Genes encoding the
213 *P4H* collagen synthases, were not dysregulated while *RRBP1* (that stimulates collagen synthesis (110)) together
214 with *PLOD1* and *PLOD2* (that stabilise collagens (111,112)) were significantly upregulated. Moreover, *SETD7*, a
215 gene known for activating collagenases (113), was significantly downregulated.

216 At the myotube stage, a fibrosis-related gene set was clearly upregulated in DMD cells, as illustrated by the
217 overexpression of *ANGPT1* (114), *CTGF* (115), collagens (*e.g.* *COL1A2* (116)), matrix metalloproteinases (*MMPs*)
218 and tissue inhibitors of metalloproteinase (*TIMPs*) (117) (Figure 5B). Conversely, the myomiR miR-133b that
219 controls *CTGF* expression (118) was repressed (Table S2). Interestingly, gene members of the transforming
220 growth factor (TGF)- β pathway, a well-known inducer of fibrosis (119), were not found dysregulated (Figure
221 5B).

222 Altogether, these data argue for fibrosis as an intrinsic feature of DMD skeletal muscle cells, rather than a
223 process solely driven by interstitial cell populations in the niche. Furthermore, this muscle-driven fibrosis
224 seems independent of the TGF- β pathway, and could rather depend on the SHH pathway, together with an
225 intrinsic upregulation of chondrocyte markers and collagens.

226 **Mitochondria, a key organelle impacted by the absence of dystrophin prior calcium dysregulation**

227 As previously described (120) and illustrated on Figure S5A, the energy metabolism of DMD hiPSC-derived
228 myotubes was dysregulated at the creatine and carbohydrate levels, up to the respiration (Figure 6A-B, Figure
229 S2C). The creatine transporter was not impacted while mRNAs coding for enzymes of both creatine and
230 creatine phosphate biosynthesis were underrepresented. Neither glucose nor glutamate transporter
231 expression were impaired. However, glutamine biosynthesis (followed by gluconeogenesis that feeds glycolysis
232 from glutamine) as well as glycogenesis (followed by glycogenolysis that feeds glycolysis from glycogen) were
233 all downregulated, together with glycolysis itself. In contrast, the pentose phosphate pathway, which is in
234 parallel to glycolysis, was upregulated, especially the oxidative part. Pyruvate decarboxylation and generation
235 of acetyl-CoA to feed the tricarboxylic acid (TCA) cycle was also impaired. Finally, the TCA cycle itself (Figure
236 6A, Figure S2C) and the mitochondrial electron transport chain were downregulated Figure 6B, Figure S2C).

237 This is particularly reinforced by lower levels of a member of the ATP synthase complex ATP5A1 at both mRNA
238 and protein levels (Figure 6C-D). Moreover, transcripts encoded by the mitochondrial DNA and mitochondrial
239 DNA itself were decreased in DMD hiPSC-derived myotubes at day 25 (Figure S5B-S5E).
240 In the presented cell model, a significant downregulation of a mRNA set coding for mitochondrial proteins was
241 primarily observed at day 10 with the downregulation of 11 % (10 mRNAs, DMD/Healthy expression ratio \leq
242 0.76, adjusted pvalue \leq 0.05) of the mitochondrial outer membrane genes, and amplified during the
243 differentiation of DMD cells (Figure 7A). Therefore, defects depicted at day 25 rooted before the expression of
244 the skeletal muscle program at day 17. Among them, mRNA downregulation of *TSPO*, a channel-like molecule
245 involved in the modulation of mitochondrial transition pore (121), occurred from day 10 to day 25. This
246 downregulation was also observed at the protein level at day 17 (Figure 7B). Moreover, the protein import
247 system was affected from day 17 at both mRNA and protein levels (Figure S5C-S5F). Simultaneously, mRNAs
248 involved in mitochondrial genome transcription started to be downregulated, followed by genes involved in
249 mitochondrial DNA replication at day 25 (Figure S5D-S5G). This progressive increase of dysregulations was also
250 observed at the level of the entire mRNA set related to mitochondria (around 1,000 mRNAs) as illustrated by
251 the volcano plots as well as the gene ontology enrichments (Figure 7C, Figure S2C).

252 Our data highlight early impairments in genes coding for mitochondria that start at the somite stage - prior
253 calcium homeostasis dysregulation - and increase with the differentiation in an orderly manner. These
254 elements complete the mitochondrial DMD phenotype described at the myotube stage.

255 Altogether, our study demonstrates that DMD starts prior to the expression of well-described markers of
256 muscle differentiation. It shows that hiPSC-based experimental models of DMD can help identify early disease
257 manifestations and stratify multiple pathological features over the course of muscle development.

258 DISCUSSION

259 Since the discovery of the *DMD* gene in 1987 (1), DMD cellular phenotypes were considered under the unique
260 scope of a “mechanical hypothesis” in which dystrophin deficiency led to membrane leakage and ultimately
261 muscle cell rupture. However, over the last 15-20 years, studies have brought unequivocal evidence that
262 multiple additional factors are in play, such as calcium intracellular overloads (122,123), excessive oxidative
263 stress (124,125), metabolic switches (126,127), as well as an overall tissue context where aberrant interactions
264 between resident cells lead to inflammation and fibro-adipogenesis (128–130). This has progressively led to a
265 complex picture involving interdependent homeostatic perturbations and to date, the identification of
266 prevalent pathological features driving the initiation of DMD is hardly feasible.

267 The skeletal myogenesis modelled here by the differentiation of hiPSCs, without gene overexpression or cell
268 sorting, homogeneously and robustly recapitulates key developmental steps – pluripotency, mesoderm,
269 somite and skeletal muscle – without any trace of other lineages. Therefore, it is a suitable dynamic model for
270 studying human skeletal muscle development in both healthy and DMD cells, offering the possibility to clarify
271 the consequences of the absence of dystrophin at each step of the differentiation process, as well as to
272 explore dystrophin functions and find earlier and more specific disease biomarkers.

273 As previously observed with pluripotent stem cells (131), hiPSC-derived myotubes at day 25 displayed an
274 embryonic/foetal gene expression profile. However, a clear distinction must be made between the nature of
275 the expressed isoforms – embryonic / foetal / postnatal – and the degree of differentiation. For instance,
276 hiPSC-derived myotubes expressed multiple markers of terminally differentiated muscles at levels higher than
277 those measured in tissue-derived myotubes. With the idea of exploring human DMD phenotypes during
278 muscle development, we argued that generating embryonic/foetal myotubes from hiPSCs would not be a
279 limitation.

280 In qualitative terms, DMD hiPSC-derived myotubes showed an overall morphology similar to healthy controls,
281 with cell fusion and clear striation patterns, suggesting that the potential impact of dystrophin during *in vitro*
282 differentiation is subtle and does not prevent myotube formation. However, our unbiased mRNA-seq analysis
283 highlighted striking transcriptome dysregulations with 3,578 differentially expressed genes at day 25. This
284 includes numerous genes which can be linked to previously described DMD phenotypes such as 1) DAPC
285 dissociation (132); 2) rupture of calcium homeostasis (122); 3) myomiR downregulation (70,133); 4) sarcomere
286 destabilisation (134–136); 5) mitochondrial and metabolism dysregulations (126,127); 6) NMJ fragmentation
287 (137,138) and 7) fibrosis (130,139). It is interesting to note that these phenotypes are already detected at the
288 transcriptional level in embryonic/foetal myotubes, while they usually appear postnatally in Human and other
289 animal models. In addition, most of them are often considered as consequences of degeneration-regeneration
290 cycles typical of DMD muscles *in vivo* (135,140,141) which are absent in our *in vitro* model, indicating that a
291 part of these defects are primarily due to the absence of dystrophin itself. In particular, our data suggest that
292 fibrosis is an intrinsic feature of DMD skeletal muscle cells, and therefore, it does not absolutely require a
293 specific tissue context or additional cell populations to be detected *in vitro*. Fibrosis is a major hallmark of
294 DMD pathophysiology, and the regulation of this process has been largely investigated in the past (119,142). A
295 long-debated question is the implication of the TGF β signalling pathway (143). In our model, TGF β signalling
296 was inhibited up to day 17 by inhibitors in the cell culture media, and TGF β -related genes were not
297 upregulated at day 25, suggesting that the observed fibrosis is TGF β - independent.

298 Since several studies on Human and other animal models had described dystrophic phenotypes in DMD
299 fetuses/infants (9–14), we investigated the precise timing of disease onset in our hiPSC-derived myotubes.
300 First, the absence of dystrophin does not modify the capacity of cells derived from adult tissue biopsies to be
301 reprogramed using the approach developed by Takeshi and Yamanaka (144). Both healthy and DMD cells
302 retained pluripotency and the capacity to enter the mesoderm compartment at day 3. At that time, the
303 embryonic dystrophin Dp412e is expressed and only marginal dysregulations are observed in DMD cells, a

304 *priori* unrelated to cell fate choice as cells only express paraxial mesoderm markers at level similar to healthy
305 controls.

306 DMD dysregulations are greatly increased at day 10, when cells express somite markers without any trace of
307 transcripts coding for the long dystrophin isoform Dp427m expressed in skeletal muscles (only the ubiquitous
308 variant Dp71-40 is found). At that time, we noticed few significant dysregulations of cell lineage markers,
309 which became more prevalent at day 17 and 25. This might be an indication that to some extent, cell fate is
310 misguided in DMD cells, where skeletal muscle markers are underexpressed and replaced by markers of
311 alternative lineages, such as chondrocytes.

312 First visible at day 10, we identified mitochondrial dysregulation as one of the key processes happening in an
313 orderly manner. Interestingly, early observations prior the discovery of the *DMD* gene had hypothesised that
314 DMD was a mitochondrial/metabolic disease based on protein quantifications and enzyme activities (126,145).
315 Later, mitochondria was identified as a key organelle in DMD, responsible for metabolic perturbations but also
316 calcium accumulation and generation of reactive oxygen species (122–125). In this study, numerous genes
317 coding for proteins located in the outer mitochondrial membrane start to be downregulated from day 10 in
318 DMD cells, such as the benzodiazepine receptor TSPO, a member of the controversial mitochondrial
319 permeability transition pore (mPTP) (121). The mPTP is a multiprotein complex whose members are not all
320 precisely identified, and several studies suggest that it might be involved in DMD pathophysiology (146,147). A
321 chicken-and-egg question currently debated relates to the initiation of these homeostatic breakdowns, as
322 positive feedbacks exist between mitochondria, oxidative stress and calcium homeostasis dysregulations
323 (123,124). In our model, dysregulations of genes controlling calcium homeostasis were detected after day 10,
324 suggesting that mitochondrial impairment starts early and has predominant consequences in DMD, as
325 hypothesised by Timpari *et al.* (120). Further experiments are needed to better evaluate the impact of
326 mitochondrial dysregulations at the functional level.

327 Day 17 marks the entry in the skeletal muscle compartment with the expression of specific transcription
328 factors, cell surface markers, the skeletal muscle variant of dystrophin (*Dp427m*), as well as myomiRs. It also
329 marks the initiation of the skeletal muscle gene dysregulations observed at the myotube stage (*i.e.*
330 downregulation of genes involved in DAPC and calcium homeostasis). For instance, the upregulation of
331 fibrosis-related genes observed in DMD myotubes at day 25 is already visible at day 17, with the upregulation
332 of the SHH pathway as well as collagen-related genes. In this study, it is seen as an early indicator of DMD
333 physiopathology, confirming previous observations in DMD infants, both transcriptionally (4) and histologically
334 (148,149).

335 Moreover, several myomiRs were found downregulated at days 17 and 25 and seem to play a central part in
336 multiple DMD phenotypes. Besides their role in myogenesis (80,81), myomiRs can be involved in calcium
337 homeostasis (150), metabolism and mitochondrial functions (151,152), and fibrosis (118,153). In particular,
338 miR-1 and miR-206 are known to target key genes such as CACNA1C (150), CTGF (118), RRB1 (153), several
339 regulators of the pentose phosphate pathway (151), and even transcripts encoded by the mitochondrial
340 genome (152). Even though the functional consequences of the multiple gene and myomiR dysregulations
341 highlighted in this study is virtually impossible to anticipate, we believe that myomiRs can be key players in
342 DMD biology.

343 Only few studies argued that DMD starts before the expression of the muscular dystrophin protein (18,154).
344 Our data supports this idea as disease phenotypes seem to be initiated at the somite stage where Dp427m was
345 not even transcribed. This could be explained by the deficit in other dystrophin isoforms expressed prior day
346 10, such as Dp412e at day 3 (15), but also by the decrease or loss of other RNA products expressed from the
347 *DMD* locus, such as the ubiquitous isoform Dp71-40 or long non-coding RNAs (155). The lack of knowledge
348 around these additional products contrasts with the extensive amount of data on the structure and function of
349 the main muscular isoform Dp427m whose most studied role is to stabilise muscle cell membrane during
350 contraction (156). Other tissue specific isoforms have been described, *e.g.* in the retina (Dp260 (30)) and in the
351 brain (Dp427c (31), Dp427p (29) and Dp140 (28)), some of which are also slightly expressed in skeletal muscles
352 under certain circumstances (157), but their role remains mostly unknown. Interestingly, in our data, the

353 expression of Dp260 follows the same pattern of expression as Dp427m. It has been shown that the expression
354 of Dp260 in *mdx/utrnK/K* mice can rescue the *mdx* phenotype (158), indicating overlapping functions between
355 Dp427m and Dp260. On the other hand, it is now well established that a third of DMD patients display
356 cognitive deficiencies – which might be correlated with mutations affecting Dp140 (159) – attesting that
357 dystrophin can be involved in other cell functions.

358 To date, the standard of care for DMD patients helps mitigate and delay some of the most severe symptoms
359 but remains insufficient to have a curative effect. Despite decades of work with the *mdx* mouse model, only a
360 few pharmacological candidate molecules have moved forward to clinical trials, with variable efficiency. As
361 several gene therapy trials have been recently initiated with promising preliminary data, we believe that our
362 human *in vitro* model system might be useful for the development of combination therapies. Recent studies
363 have proved that the association of two different therapeutic approaches could have a synergistic effect on
364 the overall treatment outcome, and can be used for instance to boost the effect of dystrophin re-expression by
365 antisense oligonucleotides or gene therapy (8,160,161). Here, our extensive RNA-seq data could help identify
366 relevant therapeutic targets for pharmacological intervention, such as CTGF – involved in fibrosis and found
367 upregulated in DMD myotubes – which can be inhibited by monoclonal antibodies (162), or TSPO receptor – a
368 receptor potentially member of the mPTP downregulated in DMD cells – targetable with benzodiazepines
369 (163). In addition, our model might also be used as a platform to screen pharmacological compounds in an
370 unbiased high-throughput manner. Indeed, skeletal muscle progenitor cells at day 17 can be robustly
371 amplified, cryopreserved and plated in a 384-well plate format (data not shown). Thus, they could be an
372 interesting tool to highlight pharmacological compounds to be used alone, or in combination with gene
373 therapy.

374 To summarise, the directed differentiation of hiPSCs without gene overexpression or cell sorting
375 homogeneously and robustly recapitulates key developmental steps of skeletal myogenesis and generates
376 embryonic/foetal myotubes without any trace of other lineages. The absence of dystrophin does not
377 compromise cell reprogramming, pluripotency or the entry into the mesoderm compartment. While none of
378 the long dystrophin isoform is expressed, a significant transcriptome dysregulation can be observed at the
379 somite stage that implicates mitochondria prior to defects in calcium homeostasis. Although being able to
380 enter the skeletal lineage compartment and become myotubes, DMD cells exhibit an imbalance in cell fate
381 choice as they express lower amount of key muscle proteins and retain basal expressions of other lineages,
382 leading to the well-characterised DMD phenotypes including muscle features and metabolism dysregulations
383 as well as fibrosis. Altogether, these data argue for 1) a deficit and not a delay in DMD differentiation; 2)
384 seeing DMD as a progressive developmental disease as well as a metabolic pathology whose onset is triggered
385 before the entry into the skeletal muscle compartment; and 3) fibrosis as an intrinsic feature of DMD muscle
386 cells. Future studies could explore the additional roles of *DMD* locus products with the impact of their loss all
387 along the skeletal muscle development, as well as find earlier and more specific disease biomarkers and
388 develop combination therapeutic strategies using high-throughput drug screening.

389 **Materials and methods**

390 **Ethics, consent, and permissions**

391 At the Cochin Hospital-Cochin Institute, the collection of primary cultures of myoblasts was established from
392 patient muscle biopsies conducted as part of medical diagnostic procedure of neuromuscular disorders. For
393 each patient included in this study, signed informed consent was obtained to collect and study biological
394 resources, and establish primary cultures of fibroblasts and myoblasts at the Hospital Cell Bank-Cochin
395 Assistance Publique—Hôpitaux de Paris (APHP). This collection of myoblasts was declared to legal and ethical
396 authorities at the Ministry of Research (number of declaration, 701, n° of the modified declaration, 701–1) via

397 the medical hosting institution, APHP, and to the “Commission Nationale de l’Informatique et des Libertés”
398 (CNIL, number of declaration, 1154515).

399 **Cells**

400 Human primary adult myoblasts from healthy individuals and DMD patients were provided by Celogos and
401 Cochin Hospital-Cochin Institute (Table S3). In Celogos laboratory, cell preparation was done according to
402 patent US2010/018873 A1.

403 **Cell culture**

404 **Human tissue-derived myoblasts** – Primary myoblasts were maintained in a myoblast medium: DMEM/F-12,
405 HEPES (31330–038, Thermo Fisher Scientific) supplemented with 10 % fetal bovine serum (FBS, Hyclone,
406 Logan, UT), 10 ng/mL fibroblast growth factor 2 (FGF2, 100-18B, Peprotech), and 50 nM Dexamethasone
407 (D4902, Sigma-Aldrich) on 0.1 % gelatin (G1393, Sigma-Aldrich) coated culture ware.

408 **Human tissue-derived myotubes** – Primary myoblasts were differentiated into myotubes. Cells were seeded at
409 600 cells/cm² on 0.1 % gelatin coated cultureware in myoblast medium containing 1 mM Acid ascorbic 2P
410 (A8960, Sigma-Aldrich).

411 **Human induced pluripotent stem cells** - Primary myoblasts were reprogrammed into hiPSCs following the
412 protocol described in (164), using the Yamanaka’s factors POU5F1, SOX2 and KLF4 transduction by ecotropic or
413 amphotropic vectors (Table S3). HiPSCs were adapted and maintained with mTeSR™1 culture medium (05850,
414 Stemcell Technologies) on Corning® Matrigel® Basement Membrane Matrix, lactose dehydrogenase elevating
415 virus (LDEV)-Free-coated cultureware (354234, Corning Incorporated). Cells were then seeded at 20,000
416 cells/cm², passaged and thawed each time with 10 μM StemMACS™ Y27632.

417 **Human iPSC-derived cell** – Six hiPSCs (3 healthy and 3 DMD) were differentiated three times toward skeletal
418 muscle lineage using commercial media designed from Caron’s work (23) (Skeletal Muscle Induction
419 medium SKM01, Myoblast Cell Culture Medium SKM02, Myotube Cell Culture Medium SKM03, AMSbio). This
420 protocol is a 2D directed differentiation that uses 3 consecutive defined media (SKM01 from day 0 to 10,
421 SKM02 from day 10 to 17 and SKM03 from day 17 to d25) and only one cell passage at day 10.

422 **DNA and RNA experiments**

423 **RNA extraction and quality** – RNA extraction was done in the six cell lines at 7 different time points: tissue-
424 derived myoblast and tissue-derived myotube, as well as during hiPSC differentiation at day 0, 3, 10, 17 and 25
425 (hiPSC-derived myotube) using the miRNeasy Mini kit (217004, QIAgen) on the QIAcube instrument. RNAs
426 coming from the part A of the extraction protocol was used for mRNA-seq and RT-qPCR. RNAs coming from the
427 part B of the extraction protocol was used for miRseq. PartA RNA was quantified on Nanodrop
428 spectrophotometer (ND-1000, Thermo Fisher Scientific) and purity/quality (RIN ≥ 7) was assessed on the 2200
429 TapeStation using the Agilent RNA ScreenTape (5067-5576 / 5067-5577 / 5067-5578, Agilent). PartB RNA was
430 quantified and purity/quality was assessed on the 2100 Agilent BioAnalyzer using the Agilent small RNA kit
431 (5067-1548, Agilent).

432 **Reverse transcription** – 500 ng of total RNA were reverse transcribed with random primers (48190–011,
433 Thermo Fisher Scientific), oligo(dT) (SO131, Thermo Fisher Scientific), and deoxynucleotide (dNTP, 10297–018,
434 Thermo Fisher Scientific) using Superscript® III reverse transcriptase (18080–044, Thermo Fisher Scientific).
435 Thermocycling conditions were 10 min, 25 °C; 60 min, 55 °C; and 15 min, 75 °C.

436 **qPCR** – We amplified cDNA/total DNA using primers (Thermo Fisher Scientific) listed in Table S4. They were
437 designed using Primer blast (<http://www.ncbi.nlm.nih.gov/tools/primer-blast>). The amplification efficiency of

438 each primer set was preliminarily determined by running a standard curve. Detection was performed using a
439 QuantStudio™ 12K Flex Real-Time PCR System (Thermo Fisher Scientific). Reactions were carried out in a 384-
440 well plate, with 10 μ L containing 2.5 μ L of 1/10 cDNA or 6.25 ng/ μ L total DNA, 0.2 μ L of mixed forward and
441 reverse primers at 10 μ M each, and 5 μ L of 2X Luminaris Color HiGreen qPCR Master Mix Low Rox (K0973,
442 Thermo Fisher Scientific). Thermocycling conditions were 50 °C during 2 min, 95 °C during 10 min, followed by
443 45 cycles including 15 sec at 95 °C, 1 min at 60 °C plus a dissociation stage. All samples were measured in
444 triplicate. Experiments were normalised using UBC as reference gene and relative quantification was done
445 with the $\Delta\Delta$ Ct method.

446 **mRNA-seq** – Libraries are prepared with TruSeq Stranded mRNA kit protocol according supplier
447 recommendations. Briefly, the key stages of this protocol are successively, the purification of PolyA containing
448 mRNA molecules using poly-T oligo attached magnetic beads from 1 μ g total RNA, a fragmentation using
449 divalent cations under elevated temperature to obtain approximately 300bp pieces, double strand cDNA
450 synthesis and finally Illumina adapter ligation and cDNA library amplification by PCR for sequencing.
451 Sequencing is then carried out on paired-end 100 b/75 b of Illumina HiSeq 4000.

452 An RNA-seq analysis workflow was designed using snakemake 3.5.4 (165) for read quality estimation, mapping
453 and differential expression analysis. Quality estimation was obtained with FastQC 0.11.5
454 (<https://www.bioinformatics.babraham.ac.uk/projects/fastqc/>). Mapping to the human genome assembly
455 Ensembl GRCh37.87 (43,695 transcripts) was performed with STAR 2.5.0a (166). According to STAR manual and
456 for more sensitive novel junction discovery, the junctions detected in a first round of mapping were used in a
457 second mapping round. Read strandness was confirmed using RSeQC (167). Expression counts at the gene
458 level were calculated using FeatureCounts 1.4.6 (168). Analysis results were summarised using MultiQC 1.0
459 (169). Normalised counts (median ratio normalisation, MRN) and differential expression analysis was
460 performed with DESeq2 1.16.1 (170), considering pairwise comparisons with all developmental stages and
461 comparing DMD versus healthy cells within developmental stages. BiomaRt 2.30.0 (171) was used to fetch
462 gene annotations from Ensembl. Transcripts with $|\log_2\text{FoldChange}| \geq 0.4$ (equivalent of DMD/healthy ratio \leq
463 0.76 or ≥ 1.32) and adjusted pvalue ≤ 0.05 were considered differentially expressed. Data are going to be
464 submitted to GEO.

465 **miRNA-seq** – 10 ng of miRNA was reverse transcribed using the Ion Total RNA-seq kit v2
466 (4475936, Thermofisher Scientific) following the protocol of the manufacturer for small RNA libraries. The
467 cDNA libraries were amplified and barcoded using Ion Total RNA-seq kit v2 and Ion Xpress RNA-seq Barcode
468 Adapters 1-16 Kit (Thermofisher Scientific). The amplicons were quantified using Agilent High Sensitivity DNA
469 kit before the samples were pooled in sets of fifteen. Emulsion PCR and Enrichment was performed on the Ion
470 OT2 system Instrument using the Ion PI Hi-Q OT2 200 kit (A26434, Thermofisher Scientific). Samples were
471 loaded on an Ion PI v3 Chip and sequenced on the Ion Proton System using Ion PI Hi-Q sequencing 200 kit
472 chemistry (200 bp read length; A26433, Thermofisher Scientific). Sequencing reads were trimmed with Prinseq
473 (172) (v0.20.4) (--trim-right 20) and filtered by average quality score (--trim-qual 20). Reads with a size less
474 than 15 bp have been removed and reads with a size greater than 100 bp have been trimmed with Cutadapt
475 (v1.16)(173). Mapping to the human genome assembly Ensembl GRCh37.87 (3111 transcripts) was performed
476 with STAR 2.5.3a (166). Normalised counts (median ratio normalisation, MRN) and differential expression
477 analysis was performed with DESeq2 1.16.1 (170), considering pairwise comparisons with all developmental
478 stages and comparing DMD versus healthy cells within developmental stages. Transcripts with
479 $|\log_2\text{FoldChange}| \geq 0.4$ (equivalent of DMD/healthy ratio ≤ 0.76 or ≥ 1.32) and pvalue ≤ 0.05 were considered
480 differentially expressed. The use of pvalue instead of adjusted pvalue is justified by biological meaning(174)
481 (i.e. well-known regulated / dysregulated miRNAs had a pvalue ≤ 0.05 but not an adjusted pvalue ≤ 0.05). Data
482 are going to be submitted to GEO.

483

484 **High-throughput data analyses** – Graphs were realised using RStudio. Viridis library (175) was used for the
485 colour palette easier to read with colour blindness and print well in grey scale. For unsupervised analyses,
486 normalised counts were standardised with scale function (center = TRUE, scale = TRUE) and plotted with
487 corrplot function from corrplot library (176). Spearman correlation was done with the cor function (method =
488 "spearman", use = "pairwise.complete.obs") on standardised data. Hierarchical clustering and heatmap were
489 performed with gplots library (177) heatmap.2 function on standardised data. Gene enrichment data were
490 retrieved from DAVID database using RDAVIDWebService library (178) on supervised list of mRNAs (mRNA-seq
491 data: adjusted pvalue ≤ 0.05 , ratio ≤ 0.76 or ≥ 1.32 , normalised counts ≥ 10 in at least one sample; enrichment
492 data: Benjamini value ≤ 0.05 , enrichment ≥ 1.5). Only Gene Ontology terms were processed.

493 **Protein experiments**

494 **Immunolabelling** – Cells (healthy hiPSC 1/ DMD hiPSC 2, Table S3) at day 17 of culture were thawed and
495 seeded at 10,000 cells/cm² in SKM02 medium in Falcon® 96-well microplate (353219, Corning) coated with
496 0.1% gelatin (G1393, Sigma-Aldrich) and 2.4 µg/mL laminin (23017015, ThermoFischer Scientific) in PBS 1X
497 (D8537, Sigma-Aldrich). After 4 days, cells were switched to DMEM/F-12, HEPES (31330038, ThermoFischer
498 Scientific) with 2% Horse serum (H1270, Sigma-Aldrich). Before staining, after removing the culture medium,
499 cells were fixed 15 min at 4°C with PFA 4% (15710, Euromedex) after 7 days of culture. A first quick Phosphate
500 buffered saline (PBS) 1X tablets (P4417, Sigma-Aldrich) wash was done, followed by another lasting 10 min.
501 Then, a solution with PBS 1X, Triton™ X-100 0.25% (T8787, Sigma-Aldrich) and Bovine serum albumin 2.5%
502 (BSA, A9418, Sigma-Aldrich) was added and incubated 30 min at room temperature. Primary antibody was
503 finally added, diluted in the same buffer (α -actinin 1/500, A7811, Sigma-Aldrich), overnight at 4°C. The next
504 day, two quick PBS 1X washes were followed by a third incubated 10 min at room temperature. An incubation
505 was done 45 min at room temperature with a mix of 4',6-Diamidino-2'-phenylindole dihydrochloride (DAPI,
506 1µg/mL, 10236276001, Sigma-Aldrich) and the secondary antibody Donkey anti-Mouse Alexa Fluor 555 in PBS
507 1X, (1/1000, A-31570, ThermoFischer Scientific). Finally, two quick PBS 1X washes were followed by a third
508 incubated 10 min at room temperature. The stained cells were kept in PBS 1X at 4°C before imaging with a
509 Zeiss LSM880 Airyscan confocal and Zen software (Black edition).

510 **Western blotting** – For tissue-derived myotubes, after three rinses with cold PBS 1X (w/o Ca²⁺ and Mg²⁺,
511 D8537, Sigma-Aldrich), protein extracts were isolated from cultured cells by scraping (O10154, Dutscher) with
512 an extraction protein buffer (NaCl 150 mM, Tris 50 mM, EDTA 10 mM (AM9260G, ThermoFischer Scientific),
513 Triton 1X, 1/100 Protease Inhibitor Cocktail (P8340, Sigma-Aldrich), PhosSTOP tablet (04906845001, Roche
514 Diagnostics)). For hiPSC-derived myotubes, cell pellets were rinsed once with cold PBS 1X, spun 5 min at 300 g
515 and resuspended in the same extraction protein buffer. Protein Extracts were centrifuged at 4°C 10 min at
516 16,000 g and supernatants were kept at -80 °C. Quantitation of total protein was done with Pierce BCA protein
517 assay kit (23225, ThermoFischer Scientific). Before gel loading, protein extracts were mixed with 9µL of loading
518 buffer (Urea 4M, SDS 3.8%, Glycerol 20%, Tris 75mM pH 6.8, 5% β -mercaptoethanol, 0.1mg/mL Bromophenol
519 blue) and completed to 28µL (for one well) with extraction protein buffer, then heated once 5 min at 95 °C.
520 Western blots were performed either with Criterion™ XT Tris-Acetate Precast Gels 3–8 % (3450130, Bio-Rad,
521 Hercules, CA), XT Tricine running buffer (161–0790, Bio-Rad) and ran at room temperature for 1 hour and 15
522 min at 150 V for RYR1 (1/1000, MA3-925, ThermoFischer Scientific), MF20 (1/500, DSHB, concentrate),
523 Manex50 (1/30, DSHB), α -sarcoglycane (1/150, A-SARC-L-CE, Leica biosystems), γ -sarcoglycane (1/150, G-
524 SARC-CE, Leica biosystems), or with 4–15% Criterion™ TGX™ Precast Midi Protein Gel (5671084, Bio-Rad), 10x
525 Tris/Glycine/SDS Running Buffer (1610772), and ran at room temperature for 1 hour at 200 V for CaV1.1
526 (1/1000, MA3-920, ThermoFischer Scientific), ATP5A (1/1,000, ab14748, ABCAM), Semaphorin 6A (1/55,
527 AF1146, R&D systems) and GLI3 (1/200, AF3690, R&D systems). Gels were rinsed once in water and blotted
528 either with “high molecular weight” or “mixed molecular weight” program of TransBlot® Turbo™ transfer
529 system (Bio-Rad) using Trans-Blot®Turbo™ Midi Nitrocellulose Transfer Packs (170–4159, Bio-Rad). Blots were
530 then processed with the SNAP i.d.® 2.0 Protein Detection System following the manufacturer’s protocol, with

531 Odyssey® Blocking Buffer (927-40003, LI-COR) for blocking and with 0,2% Tween® 20 added for antibody
532 dilutions (28829.296, VWR), washes were done with phosphate-buffered saline tween (PBST) buffer (PBS 1X
533 tablets, P4417, Sigma-Aldrich; 0.1 % Tween® 20). Every primary antibody was pooled with either α -actinin
534 (1/12,500, sc-17829, Santa Cruz or 1/7000, A7811, Sigma-Aldrich) or α -tubulin (1/6666, Ab7291, Abcam). For
535 secondary antibodies, either IRDye 800CW donkey anti-mouse and/or IRDye® 680RD donkey anti-goat were
536 used (1/5000-1/10000, 926-32212, 926-68074, LI-COR). After completion of SNAP i.d.® general protocol, with
537 the membrane still in the blot holder, two PBS 1X washes were finally done before band visualisations with
538 Odyssey® CLx Imaging System and quantification with Image Studio Lite software (Version 5.2). Statistical
539 analysis was performed using unpaired t test on GraphPad Prism software.

540 **iTRAQ proteomics –**

541 *Samples Preparation:* Cells at day 17 were collected and resuspended in 90% FBS (Hyclone), 10% DMSO
542 (A3672.0050, VWR), cooled down until -90°C with the CryoMed™ device (ThermoFisher Scientific), before
543 storage in liquid nitrogen. Cells were then thawed and washed 5 times with cold PBS and air was replaced by
544 Argon to thoroughly dry the pellet that was flash frozen in liquid nitrogen. 5-10 times the approximate cell
545 pellet volume of 0.5 M triethyl ammonium bicarbonate (TEAB) with 0.05% SDS was added to the cell pellet for
546 protein extraction. Cell pellet was re-suspended and triturated by passing through a 23-gauge needle and 1ml
547 syringe for 30 times. Samples were then sonicated on ice at amplitude of 20% for 30 x 2 sec bursts and
548 centrifuged at 16000g for 10 min at 4°C. Supernatant was transferred to a fresh Eppendorf tube. Protein was
549 quantified by nanodrop. 100-150µg of protein was aliquoted for each individual sample and 2µl TCEP (50mM
550 tris-2-carboxymethyl phosphine) was added for every 20µl of protein used for reducing the samples. After 1 hr
551 incubation at 60°C, 1µl MMTS (200mM methylmethane thiosulphonate) was added for every 20µl of protein
552 used for alkylating/'blocking' the samples. Finally, after a 10 min incubation at RT, samples were trypsinised by
553 addition of 6-7.5µl of 500ng/µl trypsin. The ration between enzyme: substrate was 1:40. Samples were
554 incubated overnight at 37°C in the dark. *iTRAQ labelling:* When iTRAQ reagents reached room temperature,
555 50µl of isopropanol/[acetonitrile] was added to each iTRAQ 8-plex reagent and was incubated at RT for 2 hrs,
556 in the dark. 8 µl of 5% hydroxylamine was added to neutralise the reaction. Each sample was separately
557 lyophilised at 45°C. Samples have been stored at -20°C or used immediately.

558 *Offline C4 High Performance Liquid Chromatography (HPLC):* All 8 samples were pooled together in 60µl of 97%
559 mobile phase A (99.92% % H₂O, 0.08% NH₄OH) and 3% mobile phase B (99.92% % Acetonitrile, 0.02% NH₄OH)
560 by serially reconstituting each sample. Extra 40µl of mobile phase was added to sample 1, after sample has
561 been well vortexed, all the contents of sample 1 tube were transferred to the tube with the sample 2 (and
562 serially repeated until all samples were pooled). Final volume of samples needed to be 100µl. After sample was
563 centrifuged at 13000g for 10 min, supernatant was collected with an HPLC injection syringe. 100µl was injected
564 onto the sample loop. Fractions were collected in a peak dependent manner. Finally, fractions were lyophilised
565 at 45°C and stored at -20°C until required. The used column was a Kromasil C4 column 100Å pore size, 3.5µm
566 particle size, 2.1mm inner diameter and 150mm length. The gradient for C4 separation was (RT in min - %B): 0-
567 3; 10-3; 11-5; 16-5; 65-20; 100-30; 15-80; 120-80; 125-3.

568 *Solid Phase Extraction Cleaning of peptides fractions:* A GracePureTMT SPE C18-Aq cartridge was used for pre-
569 cleaning of samples (Support: Silica, % Carbon: 12.5%, With endcapping, Surface area: 518m²/g, Particle size:
570 50µm, Pore size: 60Å, Water-wettable). Samples were reconstituted using in total 400µl of 1% ACN, 0.01% FA.
571 Cartridge was washed with 600µl of ACN. ACN was then completely flushed out of the column at dropwise
572 speed. This activated the ligands. Then 1% ACN, 0.01% FA (600µl) was flushed through the cartridge to
573 equilibrate the sorbent. 400µl of the sample was loaded in the cartridge. It was then very slowly flushed
574 through the cartridge and recovered into a fresh tube. This process was repeated 3 times. 2 volumes of 250µl
575 of 1%ACN, 0.01%FA were used to clean and de-salt the sample. It was flushed through very slowly. 2 volumes
576 (250µl each) were used per step (2% ACN, 10% ACN, 30% ACN, 50% ACN, 70% ACN). This cycle was repeated
577 twice. Each particular concentration was pooled in one tube. Samples were dried to dryness in a Speedvac at
578 RT overnight and stored at -20°C. Like previously, samples were pooled with 100µl of 97% mobile phase A

579 (99.92% % H₂O, 0.08% NH₄OH) and 3% mobile phase B (99.92% % Acetonitrile, 0.02% NH₄OH) and injected
580 onto the sample loop. Fractions were collected in a peak dependent manner. The gradient for SPE cleaned
581 peptides C4 separation (RT in min - %B): 0-2; 10-2; 20-5; 25-5; 35-20; 55-35; 60-35; 70-80; 75-80; 80-3.

582 *Online C18 High Precision Liquid Chromatography (HPLC)*: 30µl of loading phase (2% acetonitrile, 1.0% formic
583 acid) was added to each fraction-containing Eppendorf tube. Samples were vortexed and centrifuged. Blanks
584 (30µl mobile phase) were added into well A1 to A12. 30µl of sample 1 was pipetted into well B1, sample 2 in
585 well B2 and so on. An orthogonal 2D-LC-MS/MS analysis was performed with the Dionex Ultimate 3000 UHPLC
586 system coupled with the ultra-high-resolution nano ESI LTQ-Velos Pro Orbitrap Elite mass spectrometer
587 (Thermo Scientific).

588 *Data analysis*: HCD and CID tandem mass spectra were collected and submitted to Sequest search engine
589 implemented on the Proteome Discoverer software version 1.4 for peptide and protein identifications. All
590 spectra were searched against the UniProtKB SwissProt. The level of confidence for peptide identifications was
591 estimated using the Percolator node with decoy database searching. False discovery rate (FDR) was set to 0.05,
592 and validation was based on the q-Value. Protein ratios were normalised to protein median and peptides with
593 missing iTRAQ values were rejected from protein quantification. Phosphorylation localisation probability was
594 estimated with the phosphoRS node. Protein ratios were transformed to log₂ ratios and significant changes
595 were determined by one sample T-test. To reduce the impact of possible false positive identifications, more
596 parameters were set: 1) only proteins with more than two quantified unique peptides. 2) DMD/Healthy ratio ≥
597 1.32 or ≤ 0.76 and 3) only FDR corrected p value ≤ 0.05 were retained for bioinformatics analysis.

598 **Acknowledgements**

599 We thank the Fondation Maladies Rares (GenOmics grant), Labex Revive (Investissement d'Avenir; ANR-10-
600 LABX-73) and the AFM Téléthon for funding this project. The RNA-Sequencing libraries were processed and
601 sequenced by Integragen (Evry, France). We gratefully acknowledge support from the PSMN (Pôle Scientifique
602 de Modélisation Numérique) of the ENS de Lyon for the computing resources. We thank Dr Nacira Tabti, Dr
603 Elisabeth Le Rumeur, Dr Nathalie Deburgrave and Dr Malgorzata Rak for providing us with specific reagents
604 and antibodies. We thank Dr David Israeli for his feedback on the manuscript and overall discussion on our
605 project.

606 Figure legends

607 **Figure 1 – Differentiation dynamics of hiPSCs (D0) into MyoT (D25) in healthy cells at the transcriptomic**
608 **levels. A)** Spearman correlation matrix of transcriptomes (mRNAs, right) and miRNomes (miRNAs, left). Yellow
609 dots indicate a stronger correlation. **B)** Heatmap of selected differentiation markers. (D: day; hiPSC: human
610 induced pluripotent stem cell; MyoT: myotube).

611 **Figure 2 – Differentiation dynamics of hiPSCs (D0) into MyoT (D25) in DMD cells. A)** Dotplot of DMD/healthy
612 expression ratios of selected markers. Statistical differences are indicated in brackets after gene names, and
613 grey circles around the corresponding dots. **B)** Proportions of significantly dysregulated mRNAs (adjusted
614 pvalue ≤ 0.05) in DMD cells at each time points. Expression of **C)** hsa-miR-1 and **D)** ATP2A2 mRNA during
615 differentiation, as well as **E)** ATP2A2 protein level at D17. (*adjusted pvalue ≤ 0.05 , **adjusted pvalue ≤ 0.01 ,
616 ***adjusted pvalue ≤ 0.001 , ****adjusted pvalue ≤ 0.0001 ; D: day; hiPSC: human induced pluripotent stem
617 cell; MyoT: myotube).

618 **Figure 3 – Comparison of healthy and DMD MyoT from hiPSCs and tissues at the protein level. A)** hiPSC-
619 derived MyoT immunolabelling of α -actinin (red) and nuclei (DAPI, blue) in healthy (left) and DMD cells (right).
620 **B)** Representative Western blots and related quantifications of DMD, SGCA, SGCG, myosin heavy chains,
621 CACNA1S and RYR1 from protein extracts in healthy and DMD hiPSC-derived and tissue-derived MyoT (X: 0.25
622 μg of total protein was used in hiPSC-derived MyoT instead of 7 μg in tissue-derived MyoT - *pvalue ≤ 0.05 ,
623 **pvalue ≤ 0.01 , ***pvalue ≤ 0.001 , ****pvalue ≤ 0.0001). (hiPSC: human induced pluripotent stem cell;
624 MyoT: myotube).

625 **Figure 4 – Manifestation of the DMD phenotype in the transcriptomes and miRNomes of myotubes derived**
626 **from hiPSCs and tissues. A)** Hierarchical clustering and heatmap in healthy hiPSCs (D0), hiPSC-derived MyoT
627 and tissue-derived MyoT with selected skeletal muscle transcripts and miRNAs. **B)** Volcano plots of
628 dysregulated mRNAs/miRNAs in hiPSC-derived MyoT (left) and tissue-derived MyoT (right) – vertical grey
629 dashed lines represent DMD/Healthy ratio thresholds at 0.76 or 1.32 - the horizontal grey dashed line
630 represents the adjusted pvalue threshold at 0.05. (DAPC: dystrophin-associated protein complex; hiPSC:
631 human induced pluripotent stem cell; MyoT: myotube; NMJ: neuromuscular junction; TF: transcription factor).

632 **Figure 5 – Illustration of the fibrosis phenotypes in DMD cells. Volcano plots of dysregulated mRNAs/miRNAs**
633 **related to A)** the SHH pathway and collagen metabolism at D10/17/25; and **B)** fibrosis at D25 – vertical grey
634 dashed lines represent DMD/Healthy ratio thresholds at 0.76 or 1.32 - the horizontal grey dashed line
635 represents the adjusted pvalue threshold at 0.05. (D: day; MMP: matrix metalloproteinase; SHH: sonic
636 hedgehog pathway; TIMP: tissue inhibitor of metalloproteinase; TGF: transforming growth factor).

637 **Figure 6 – Illustration of the metabolic and mitochondrial phenotypes in DMD cells. Volcano plots of**
638 **dysregulated mRNAs/miRNAs related to A)** principal metabolic pathways; and **B)** the constitution of the five
639 mitochondrial respiratory complexes in DMD hiPSC-derived MyoT – vertical grey dashed lines represent
640 DMD/Healthy ratio thresholds at 0.76 or 1.32 - the horizontal grey dashed line represents the adjusted pvalue
641 threshold at 0.05. Quantification of ATP5A1 expression **C)** at the mRNA level during differentiation, and **D)** at
642 the protein level at D17 (iTRAQ data, left) and D25 (Western blot data, right). (*adjusted pvalue ≤ 0.05 ,
643 **adjusted pvalue ≤ 0.01 , ***adjusted pvalue ≤ 0.001 , ****adjusted pvalue ≤ 0.0001). (D: day; hiPSC: human
644 induced pluripotent stem cell, MyoT: myotube)

645 **Figure 7 – Mitochondrial dysregulations in DMD cells during differentiation. A)** Absolute (top) and relative
646 numbers (% , bottom) of dysregulated genes from the different mitochondrial compartments over the course
647 of DMD hiPSC differentiation. **B)** Expression ratios of selected mitochondrial proteins. Statistical differences
648 are indicated in brackets (*adjusted pvalue ≤ 0.05 , **adjusted pvalue ≤ 0.01 , ***adjusted pvalue ≤ 0.001 ,
649 ****adjusted pvalue ≤ 0.0001). **C)** Volcano plots of mitochondria-related genes over the course of DMD hiPSC

650 differentiation. Statistical differences are symbolised with orange dots – vertical grey dashed lines represent
651 DMD/Healthy ratio thresholds at 0.76 or 1.32 - the horizontal grey dashed line represents the adjusted pvalue
652 threshold at 0.05 – The percentage of significantly dysregulated genes is indicated at the bottom right in grey.
653 (D: day).

654 **Figure S1 – DMD variant expression over the course of hiPSC differentiation. A)** Bright field microscope
655 pictures at the 7 differentiation points giving rise to hiPSC-derived and tissue-derived MyoT. Possible
656 cryopreservation time points are indicated by snowflakes. **B)** RT-qPCR relative quantification of *DMD* variants
657 expression during differentiation of hiPSCs (D0) into MyoT (D25) with the related cycle threshold (CT) values
658 (Ct: cycle threshold; D: day; hiPSC: human induced pluripotent stem cell; MyoB: myoblast; MyoT: myotube).

659 **Figure S2 – Gene ontology enrichments over the course of healthy and DMD hiPSC differentiation A)**
660 Proportions of significantly regulated mRNAs (adjusted pvalue ≤ 0.01) between successive differentiation time
661 points during the differentiation of healthy hiPSCs. Gene ontology enrichments on **B)** significantly regulated
662 mRNAs between successive differentiation time points in healthy cells (number of genes in brackets) and **C)**
663 significantly dysregulated mRNAs at each differentiation time points in DMD cells. The number of genes
664 involved in these significant enrichments is indicated in brackets next to each GO term. In green, GO terms
665 related to downregulated genes and in yellow, GO terms related to upregulated genes and in yellow (BP:
666 biological process; CC: cellular component; D: day; hiPSC: human induced pluripotent stem cell; MyoT:
667 myotube).

668 **Figure S3 – Comparison of healthy and DMD cells at D10 and D17, protein analyses.** Western blots and
669 quantifications of **A)** SEMA6A at D10, **B)** GLI3 at D10 and **C)** GLI3 at D17. (*pvalue ≤ 0.05 , **pvalue ≤ 0.01 ,
670 ***pvalue ≤ 0.001 , ****pvalue ≤ 0.0001 ; D: day; GLI3FL: GLI3 full length; GLI3R: GLI3 repressor).

671 **Figure S4 – Comparison of hiPSC-derived and tissue-derived MyoT for the expression of cell cycle genes and**
672 **myogenic regulators.** Hierarchical clustering and heatmap of **A)** selected cell cycle transcripts and miRNAs, and
673 **B)** DLK1, IGF2 and selected myosin transcripts in hiPSCs (D0), hiPSC- and tissue-derived MyoT. **C)** Dotplot of
674 DMD/healthy expression ratio of muscle transcription factors. Significant statistical differences are shown in
675 brackets (*adjusted pvalue ≤ 0.05 , **adjusted pvalue ≤ 0.01 , ***adjusted pvalue ≤ 0.001 , ****adjusted pvalue
676 ≤ 0.0001) . (hiPSC: human induced pluripotent stem cell; MyoT: myotube).

677 **Figure S5 – Dysregulations of metabolic pathways and mitochondrial genes during differentiation of DMD**
678 **hiPSCs. A)** Scheme of metabolism dysregulations at day 25. Dotplots of **B)** mitochondrial transcripts, **C)**
679 transcripts coding mitochondrial protein import, and **D)** transcripts coding mitochondrial
680 transcription/replication; **E)** Mitochondrial DNA quantification by RT-qPCR at D25. Dotplots of mitochondrial
681 proteins expressed at D17 involved in **F)** protein import, **G)** mitochondrial transcription/replication. Statistics
682 are in brackets (*adjusted pvalue ≤ 0.05 , **adjusted pvalue ≤ 0.01 , ***adjusted pvalue ≤ 0.001 , ****adjusted
683 pvalue ≤ 0.0001 ; D: day).

684 **References**

- 685 1. Hoffman EP, Brown RH, Kunkel LM. Dystrophin: the protein product of the Duchenne muscular dystrophy locus. *Cell*. 1987;51(6):919–28.
- 687 2. Koeks Z, Bladen CL, Salgado D, van Zwet E, Pogoryelova O, McMacken G, et al. Clinical Outcomes in Duchenne Muscular Dystrophy: A Study of 5345 Patients from the TREAT-NMD DMD Global Database. *J Neuromuscul Dis [Internet]*. 2017;4(4):293–306. Available from: <http://www.ncbi.nlm.nih.gov/pubmed/29125504><http://www.pubmedcentral.nih.gov/articlerender.fcgi?artid=PMC5701764>
- 691 3. Liu M, Chino N, Ishihara T. Muscle damage progression in Duchenne muscular dystrophy evaluated by a new quantitative computed tomography method. *Arch Phys Med Rehab*. 1993;74(5):507–14.
- 693 4. Pescatori M, Broccolini A, Minetti C, Bertini E, Bruno C, D’amico A, et al. Gene expression profiling in the early phases of {DMD:} a constant molecular signature characterizes {DMD} muscle from early postnatal life throughout disease progression. *{FASEB} J*. 2007;21(4):1210–26.
- 696 5. Szigyarto C, Spitali P. Biomarkers of Duchenne muscular dystrophy: current findings. *Degener Neurol Neuromuscul Dis*. 2018;8:1–13.
- 698 6. Moat SJ, Bradley DM, Salmon R, Clarke A, Hartley L. Newborn bloodspot screening for Duchenne muscular dystrophy: 21 years experience in Wales {{UK}}. *Eur J Hum Genet*. 2013;21(10):1049–53.
- 700 7. Crone M, Mah JK. Current and Emerging Therapies for Duchenne Muscular Dystrophy. *Curr Treat Options Neurol*. 2018;20(8):31.
- 701 8. Ngoc L-N, Malerba A, Popplewell L, Schnell F, Hanson G, Dickson G. Systemic Antisense Therapeutics for Dystrophin and Myostatin Exon Splice Modulation Improve Muscle Pathology of Adult mdx Mice. *Mol Ther - Nucleic Acids*. 2017;6:15–28.
- 703 9. Nguyen F, Cheral Y, Guigand L, I G-L, Wyers M. Muscle lesions associated with dystrophin deficiency in neonatal golden retriever puppies. *J Comp Pathol*. 2002;126(2–3):100–8.
- 705 10. Bassett DI. Dystrophin is required for the formation of stable muscle attachments in the zebrafish embryo. *Development*. 2003;130(23):5851–60.
- 707 11. Merrick D, Stadler LK, Larner D, Smith J. Muscular dystrophy begins early in embryonic development deriving from stem cell loss and disrupted skeletal muscle formation. *Dis Model Mech*. 2009;2(7–8):374–88.
- 709 12. Emery AE. Muscle histology and creatine kinase levels in the foetus in Duchenne muscular dystrophy. *Nature*. 1977;266(5601):472–3.
- 711 13. Toop J, Emery AE. Muscle histology in fetuses at risk for Duchenne muscular dystrophy. *Clin Genet*. 1974;5(3):230–3.
- 712 14. Vassilopoulos D, Emery AE. Muscle nuclear changes in fetuses at risk for Duchenne muscular dystrophy. *J Med Genet*. 1977;14(1):13–5.
- 714 15. Massouridès E, Polentes J, Mangeot PE, Mournetas V, Nectoux J, Deburgrave N, et al. Dp412e: A novel human embryonic dystrophin isoform induced by BMP4 in early differentiated cells. *Skelet Muscle [Internet]*. 2015 Dec 14 [cited 2017 Feb 27];5(1):40. Available from: <http://www.skeletalmusclejournal.com/content/5/1/40>
- 717 16. Nesmith AP, Wagner MA, Pasqualini FS, B OB, Pincus MJ, August PR, et al. A human in vitro model of Duchenne muscular dystrophy muscle formation and contractility. *J Cell Biol*. 2016;215(1):47–56.
- 719 17. Shoji E, Sakurai H, Nishino T, Nakahata T, Heike T, Awaya T, et al. Early pathogenesis of Duchenne muscular dystrophy modelled in patient-derived human induced pluripotent stem cells. *Sci Rep*. 2015;5:12831.
- 721 18. Choi IY, Lim HT, Estrellas K, Mula J, Cohen T V., Zhang Y, et al. Concordant but Varied Phenotypes among Duchenne Muscular Dystrophy Patient-Specific Myoblasts Derived using a Human iPSC-Based Model. *Cell Rep*. 2016;15(10):2301–12.
- 723 19. Chal J, Oginuma M, Al Tanoury Z, Gobert B, Sumara O, Hick A, et al. Differentiation of pluripotent stem cells to muscle fiber to model Duchenne muscular dystrophy. *Nat Biotechnol*. 2015;33(9):962–9.
- 725 20. Young CS, Hicks MR, Ermolova N V, Nakano H, Jan M, Younesi S, et al. A Single {CRISPR-Cas9} Deletion Strategy that Targets the Majority of {DMD} Patients Restores Dystrophin Function in {hiPSC-Derived} Muscle Cells. *Cell Stem Cell*. 2016;18(4):533–40.
- 727 21. Hicks MR, Hiserodt J, Paras K, Fujiwara W, Eskin A, Jan M, et al. {ERBB3} and {NGFR} mark a distinct skeletal muscle progenitor cell in human development and {hPSCs}. *Nat Cell Biol*. 2018;20(1):46–57.
- 729 22. Kodaka Y, Rabu G, Asakura A. Skeletal Muscle Cell Induction from Pluripotent Stem Cells. *Stem Cells Int*. 2017;2017:1376151.
- 730 23. Caron L, Kher D, Lee KL, McKernan R, Dumevska B, Hidalgo A, et al. A Human Pluripotent Stem Cell Model of Facioscapulohumeral Muscular Dystrophy-Affected Skeletal Muscles. *Stem Cells Transl Med*. 2016;5(9):1145–61.
- 732 24. Shelton M, Metz J, Liu J, Carpenedo RL, Demers S-PP, Stanford WL, et al. Derivation and expansion of {PAX7-positive} muscle progenitors from human and mouse embryonic stem cells. *Stem Cell Reports*. 2014;3(3):516–29.
- 734 25. Xi H, Fujiwara W, Gonzalez K, Jan M, Liebscher S, Van Handel B, et al. {In~Vivo} Human Somitogenesis Guides Somite Development from {hPSCs}. *Cell Rep*. 2017;18(6):1573–85.
- 736 26. Monaco AP, Neve RL, Chris C-F, Bertelson CJ, Kurnit DM, Kunkel LM. Isolation of candidate {cDNAs} for portions of the Duchenne muscular dystrophy gene. *Nature*. 1986;323(6089):646–50.
- 737

- 738 27. Byers TJ, Lidov HGW, Kunkel LM. An alternative dystrophin transcript specific to peripheral nerve. *Nat Genet.* 1993;4(1):ng0593-77.
739
- 740 28. Lidov HG, Selig S, Kunkel LM. Dp140: a novel 140 {kDa} {CNS} transcript from the dystrophin locus. *Hum Mol Genet.* 1995;4(3):329–35.
741
- 742 29. Górecki DC, Monaco AP, Derry JM, Walker AP, Barnard EA, Barnard PJ. Expression of four alternative dystrophin transcripts in brain regions regulated by different promoters. *Hum Mol Genet.* 1992;1(7):505–10.
743
- 744 30. D'souza VN, Man NT, Morris GE, Karges W, Pillers DAM, Ray PN. A novel dystrophin isoform is required for normal retinal electrophysiology. *Hum Mol Genet.* 1995;4(5):837–42.
745
- 746 31. Nudel U, Zuk D, Einat P, Zeelon E, Levy Z, Neuman S, et al. Duchenne muscular dystrophy gene product is not identical in muscle and brain. *Nature.* 1989;337(6202):337076a0.
747
- 748 32. Heikinheimo M, Scandrett JM, Wilson DB. Localization of Transcription Factor GATA-4 to Regions of the Mouse Embryo Involved in Cardiac Development. *Dev Biol.* 1994;164(2):361–73.
749
- 750 33. Lyons I, Parsons LM, Hartley L, Li R, Andrews JE, Robb L, et al. Myogenic and morphogenetic defects in the heart tubes of murine embryos lacking the homeo box gene Nkx2-5. *Genes Dev.* 1995;9(13):1654–66.
751
- 752 34. Pfeffer PL, Gerster T, Lun K, Brand M, Busslinger M. Characterization of three novel members of the zebrafish Pax2/5/8 family: dependency of Pax5 and Pax8 expression on the Pax2.1 (noi) function. *Development [Internet].* 1998;125(16):3063–74. Available from: <http://www.ncbi.nlm.nih.gov/pubmed/9671580>
753
754
- 755 35. So P, Danielian PS. Cloning and expression analysis of a mouse gene related to Drosophila odd-skipped. *Mech Dev.* 1999;84(1–2):157–60.
756
- 757 36. Hancock SN, Agulnik SI, Silver LM, Papaioannou VE, Lowe LA, Yamada S, et al. Mapping and expression analysis of the mouse ortholog of Xenopus Eomesodermin. *Mech Dev.* 1999;81(1–2):205–8.
758
- 759 37. Chapman DL, Cooper-Morgan A, Harrelson Z, Papaioannou VE. Critical role for Tbx6 in mesoderm specification in the mouse embryo. *Mech Dev.* 2003;120(7):837–47.
760
- 761 38. Lowe LA, Yamada S, Kuehn MR. Genetic dissection of nodal function in patterning the mouse embryo. *Development [Internet].* 2001;128(10):1831–43. Available from: <http://www.ncbi.nlm.nih.gov/pubmed/11311163>
762
- 763 39. Hart AH, Hartley L, Sourris K, Stadler ES, Li R, Stanley EG, et al. Mixl1 is required for axial mesendoderm morphogenesis and patterning in the murine embryo. *Development [Internet].* 2002;129(15):3597–608. Available from: <http://www.ncbi.nlm.nih.gov/pubmed/12117810>
764
765
- 766 40. Kwon GS, Fraser ST, Eakin GS, Mangano M, Isern J, Sahr KE, et al. Tg(Afp-GFP) expression marks primitive and definitive endoderm lineages during mouse development. *Dev Dyn.* 2006;235(9):2549–58.
767
- 768 41. Kanai-Azuma M, Kanai Y, Gad JM, Tajima Y, Taya C, Kurohmaru M, et al. Depletion of definitive gut endoderm in Sox17-null mutant mice. *Development [Internet].* 2002;129(10):2367–79. Available from: <http://www.ncbi.nlm.nih.gov/pubmed/11973269>
769
- 770 42. Zhang X, Huang CT, Chen J, Pankratz MT, Xi J, Li J, et al. Pax6 is a human neuroectoderm cell fate determinant. *Cell Stem Cell.* 2010;7(1):90–100.
771
- 772 43. Rex M, Orme A, Uwanogho D, Tointon K, Wigmore PM, Sharpe PT, et al. Dynamic expression of chicken Sox2 and Sox3 genes in ectoderm induced to form neural tissue. *Dev Dyn.* 1997;209(3):323–32.
773
- 774 44. Machon O, Masek J, Machonova O, Krauss S, Kozmik Z. Meis2 is essential for cranial and cardiac neural crest development. *BMC Dev Biol.* 2015;15(1):40.
775
- 776 45. Laing NG, Dye DE, Wallgren-Pettersson C, Richard G, Monnier N, Lillis S, et al. Mutations and polymorphisms of the skeletal muscle α -actin gene (ACTA1). *Hum Mutat.* 2009;30(9):1267–77.
777
- 778 46. Kardon G, Heanue TA, Tabin CJ. Pax3 and Dach2 positive regulation in the developing somite. *Dev Dyn.* 2002;224(3):350–5.
779
- 779 47. Pereira FA, Yuhong Q, Zhou G, Tsai MJ, Tsai SY. The orphan nuclear receptor COUP-TFII is required for angiogenesis and heart development. *Genes Dev.* 1999;13(8):1037–49.
780
- 781 48. Mitsiadis TA, Salmivirta M, Muramatsu T, Muramatsu H, Rauvala H, Lehtonen E, et al. Expression of the heparin-binding cytokines, midkine (MK) and HB-GAM (pleiotrophin) is associated with epithelial-mesenchymal interactions during fetal development and organogenesis. *Development [Internet].* 1995;121(1):37–51. Available from: <http://www.ncbi.nlm.nih.gov/pubmed/7867507>
782
783
784
- 785 49. Yang XM, Vogan K, Gros P, Park M. Expression of the met receptor tyrosine kinase in muscle progenitor cells in somites and limbs is absent in Splotch mice. *Development [Internet].* 1996;122(7):2163–71. Available from: <http://www.ncbi.nlm.nih.gov/pubmed/8681797>
786
787
- 788 50. Sasaki H, Ferguson-Smith AC, Shum AS, Barton SC, Surani MA. Temporal and spatial regulation of H19 imprinting in normal and uniparental mouse embryos. *Development [Internet].* 1995;121(12):4195–202. Available from: <http://www.ncbi.nlm.nih.gov/pubmed/8575319>
789
790
- 791 51. Borycki AG, Mendham L, Emerson CP. Control of somite patterning by Sonic hedgehog and its downstream signal response genes. *Development [Internet].* 1998;125(4):777–90. Available from: <http://www.ncbi.nlm.nih.gov/pubmed/9435297>
792
- 793 52. Lee CS, Buttitta L, Fan C-M. Evidence that the {WNT-inducible} growth arrest-specific gene 1 encodes an antagonist of sonic
793

- 794 hedgehog signaling in the somite. *Proc Natl Acad Sci.* 2001;98(20):11347–52.
- 795 53. McMahon AR, Merzdorf CS. Expression of the *zic1*, *zic2*, *zic3*, and *zic4* genes in early chick embryos. *BMC Res Notes.*
796 2010;3(1):167.
- 797 54. Bladt F, Riethmacher D, Isenmann S, Aguzzi A, Birchmeier C. Essential role for the c-met receptor in the migration of myogenic
798 precursor cells into the limb bud. *Nature.* 1995;376(6543):768–71.
- 799 55. Swartz ME, Eberhart J, Pasquale EB, Krull CE. EphA4/ephrin-A5 interactions in muscle precursor cell migration in the avian
800 forelimb. *Development [Internet].* 2001;128(23):4669–80. Available from: <http://www.ncbi.nlm.nih.gov/pubmed/11731448>
- 801 56. Schäfer K, Braun T. Early specification of limb muscle precursor cells by the homeobox gene *Lbx1h*. *Nat Genet.*
802 1999;23(2):ng1099_213.
- 803 57. Jeong Kyo Yoon, Wold B. The bHLH regulator pMesogenin1 is required for maturation and segmentation of paraxial mesoderm.
804 *Genes Dev.* 2000;14(24):3204–14.
- 805 58. Crossley PH, Minowada G, MacArthur CA, Martin GR. Roles for FGF8 in the induction, initiation, and maintenance of chick limb
806 development. *Cell.* 1996;84(1):127–36.
- 807 59. Brugmann SA. Six1 promotes a placodal fate within the lateral neurogenic ectoderm by functioning as both a transcriptional
808 activator and repressor. *Development.* 2004;131(23):5871–81.
- 809 60. Stewart RA, Arduini BL, Berghmans S, George RE, Kanki JP, Henion PD, et al. Zebrafish *foxd3* is selectively required for neural
810 crest specification, migration and survival. *Dev Biol.* 2006;292(1):174–88.
- 811 61. Deutsch U, Dressler GR, Gruss P. Pax 1, a member of a paired box homologous murine gene family, is expressed in segmented
812 structures during development. *Cell.* 1988;53(4):617–25.
- 813 62. Neubüser A, Koseki H, Balling R. Characterization and developmental expression of Pax9, a paired-box-containing gene related to
814 Pax1. *Dev Biol.* 1995;170(2):701–16.
- 815 63. Buchner G, Broccoli V, Bulfone A, Orfanelli U, Gattuso C, Ballabio A, et al. {MAEG,} an {EGF-repeat} containing gene, is a new
816 marker associated with dermatome specification and morphogenesis of its derivatives. *Mech Dev.* 2000;98(1–2):179–82.
- 817 64. Xu X-M, Fisher DA, Zhou L, White FA, Ng S, Snider WD, et al. The Transmembrane Protein Semaphorin {6A} Repels Embryonic
818 Sympathetic Axons. *J Neurosci.* 2000;20(7):2638–48.
- 819 65. Davis RL, Weintraub H, Lassar AB. Expression of a single transfected cDNA converts fibroblasts to myoblasts. *Cell.*
820 1987;51(6):987–1000.
- 821 66. Donalies M, Cramer M, Ringwald M, A S-P. Expression of M-cadherin, a member of the cadherin multigene family, correlates
822 with differentiation of skeletal muscle cells. *Proc Natl Acad Sci.* 1991;88(18):8024–8.
- 823 67. Gahlmann R, Kedes L. Cloning, structural analysis, and expression of the human fast twitch skeletal muscle troponin C gene. *J*
824 *Biol Chem.* 1990;265(21):12520–8.
- 825 68. Roberds SL, Anderson RD, Ibraghimov-Beskrovnya O, Campbell KP. Primary structure and muscle-specific expression of the 50-
826 kDa dystrophin-associated glycoprotein (adhelin). *J Biol Chem [Internet].* 1993;268(32):23739–42. Available from:
827 <http://www.ncbi.nlm.nih.gov/pubmed/8226900>
- 828 69. MacKenzie AE, Korneluk RG, Zorzato F, Fujii J, Phillips M, Iles D, et al. The human ryanodine receptor gene: its mapping to
829 19q13.1, placement in a chromosome 19 linkage group, and exclusion as the gene causing myotonic dystrophy. *Am J Hum Genet*
830 *[Internet].* 1990;46(6):1082–9. Available from:
831 <http://www.ncbi.nlm.nih.gov/pubmed/1971150><http://www.pubmedcentral.nih.gov/articlerender.fcgi?artid=PMC1683814>
- 832 70. Greco S, De Simone M, Colussi C, Zaccagnini G, Fasanaro P, Pescatori M, et al. Common {micro-RNA} signature in skeletal muscle
833 damage and regeneration induced by Duchenne muscular dystrophy and acute ischemia. *{FASEB} J.* 2009;23(10):3335–46.
- 834 71. Millet C, Duprez D. The Mxk homeoprotein promotes tenogenesis in stem cells and improves tendon repair. *Ann Transl Med.*
835 2015;3(Suppl 1):S33.
- 836 72. Brent AE, Schweitzer R, Tabin CJ. A somitic compartment of tendon progenitors. *Cell.* 2003;113(2):235–48.
- 837 73. Lefebvre V, Li P, De Crombrughe B. A new long form of Sox5 (L-Sox5), Sox6 and Sox9 are coexpressed in chondrogenesis and
838 cooperatively activate the type II collagen gene. *EMBO J.* 1998;17(19):5718–33.
- 839 74. Gao Y, Jheon A, Nourkeyhani H, Kobayashi H, Ganss B. Molecular cloning, structure, expression, and chromosomal localization of
840 the human Osterix (SP7) gene. *Gene.* 2004;341(1–2):101–10.
- 841 75. NODA M, DENHARDT DT. Regulation of Osteopontin Gene Expression in Osteoblasts. *Ann N Y Acad Sci.* 1995;760(1):242–8.
- 842 76. Kobayashi A, Valerius MT, Mugford JW, Carroll TJ, Self M, Oliver G, et al. Six2 Defines and Regulates a Multipotent Self-Renewing
843 Nephron Progenitor Population throughout Mammalian Kidney Development. *Cell Stem Cell.* 2008;3(2):169–81.
- 844 77. Atala A. Re: Sall1 Maintains Nephron Progenitors and Nascent Nephrons by Acting as Both an Activator and a Repressor: Editorial
845 Comment. *J Urol.* 2015;194(2):592–3.
- 846 78. Lytton J, DH M. Molecular cloning of {cDNAs} from human kidney coding for two alternatively spliced products of the cardiac
847 {Ca2+-ATPase} gene. *J Biol Chem.* 1988;263(29):15024–31.

- 848 79. Yoshida M, Ozawa E. Glycoprotein complex anchoring dystrophin to sarcolemma. *J Biochem.* 1990;108(5):748–52.
- 849 80. Chen JF, Mandel EM, Thomson JM, Wu Q, Callis TE, Hammond SM, et al. The role of microRNA-1 and microRNA-133 in skeletal
850 muscle proliferation and differentiation. *Nat Genet.* 2006;38(2):228–33.
- 851 81. Hak KK, Yong SL, Sivaprasad U, Malhotra A, Dutta A. Muscle-specific microRNA miR-206 promotes muscle differentiation. *J Cell
852 Biol.* 2006;174(5):677–87.
- 853 82. Hasty P, Bradley A, Morris JH, Edmondson DG, Venuti JM, Olson EN, et al. Muscle deficiency and neonatal death in mice with a
854 targeted mutation in the myogenin gene. *Nature.* 1993;364(6437):364501a0.
- 855 83. Vignier N, Moghadaszadeh B, Gary F, Beckmann J, Mayer U, Guicheney P. Structure, genetic localization, and identification of the
856 cardiac and skeletal muscle transcripts of the human integrin $\alpha 7$ gene (ITGA7). *Biochem Biophys Res Commun.* 1999;260(2):357–
857 64.
- 858 84. Newey SE, Howman E V., Ponting CP, Benson MA, Nawrotzki R, Loh NY, et al. Syncoilin, a Novel Member of the Intermediate
859 Filament Superfamily That Interacts with α -Dystrobrevin in Skeletal Muscle. *J Biol Chem.* 2001;276(9):6645–55.
- 860 85. WU Q-L, JHA PK, RAYCHOWDHURY MK, DU Y, LEAVIS PC, SARKAR S. Isolation and Characterization of Human Fast Skeletal β
861 Troponin T cDNA: Comparative Sequence Analysis of Isoforms and Insight into the Evolution of Members of a Multigene Family.
862 *DNA Cell Biol.* 2009;13(3):217–33.
- 863 86. Bernick EP, Zhang PJ, Du S. Knockdown and overexpression of Unc-45b result in defective myofibril organization in skeletal
864 muscles of zebrafish embryos. *BMC Cell Biol.* 2010;11(1):70.
- 865 87. Li H, Randall WR, Du S-J. skNAC (skeletal Naca), a muscle-specific isoform of Naca (nascent polypeptide-associated complex
866 alpha), is required for myofibril organization. *FASEB J.* 2009;23(6):1988–2000.
- 867 88. DeChiara TM, Bowen DC, Valenzuela DM, Simmons M V., Poueymirou WT, Thomas S, et al. The receptor tyrosine kinase MuSK is
868 required for neuromuscular junction formation in vivo. *Cell.* 1996;85(4):501–12.
- 869 89. Okada K, Inoue A, Okada M, Murata Y, Kakuta S, Jigami T, et al. The Muscle Protein Dok-7 Is Essential for Neuromuscular
870 Synaptogenesis. *Science (80-).* 2006;312(5781):1802–5.
- 871 90. Ilene K-M, Travis M, Blau H, Leinwand LA. Expression and {DNA} sequence analysis of a human embryonic skeletal muscle mvosin
872 heavy chain gene. *Nucleic Acids Res.* 1989;17(15):6167–79.
- 873 91. Weiss A, Schiaffino S, Leinwand LA. Comparative sequence analysis of the complete human sarcomeric myosin heavy chain
874 family: implications for functional {diversity11Edited} by J. Karn. *J Mol Biol.* 1999;290(1):61–75.
- 875 92. Strohman RC, J M-E, Glass CA, Matsuda R. Human fetal muscle and cultured myotubes derived from it contain a fetal-specific
876 myosin light chain. *Science (80-).* 1983;221(4614):955–7.
- 877 93. Collins C, Hayden MR, Schappert K. The genomic organization of a novel regulatory myosin light chain gene (MYL5) that maps to
878 chromosome 4p16.3 and shows different patterns of expression between primates. *Hum Mol Genet.* 1992;1(9):727–33.
- 879 94. Type Iix myosin heavy chain transcripts are expressed in type IIb fibers of human skeletal muscle. *Am J Physiol - Cell Physiol.*
880 1994;267(6 36-6):C1723-8.
- 881 95. Rotwein P, Pollock KM, Watson M, Milbrandt JD. Insulin-like growth factor gene expression during rat embryonic development.
882 *Endocrinology.* 1987;121(6):2141–4.
- 883 96. Andersen DC, Laborda J, Baladron V, Kassem M, Sheikh SP, Jensen CH. Dual role of delta-like 1 homolog (DLK1) in skeletal muscle
884 development and adult muscle regeneration. *Development.* 2013;140(18):3743–53.
- 885 97. Noguchi S, EM M, Othmane BK, Hagiwara Y, Mizuno Y, Yoshida M, et al. Mutations in the dystrophin-associated protein gamma-
886 sarcoglycan in chromosome 13 muscular dystrophy. *Sci New York N Y.* 1995;270(5237):819–22.
- 887 98. Campbell KP, Leung AT, Sharp AH. The biochemistry and molecular biology of the dihydropyridine-sensitive calcium channel.
888 *Trends Neurosci.* 1988;11(10):425–30.
- 889 99. A fourth human MEF2 transcription factor, hMEF2D, is an early marker of the myogenic lineage. *Development.*
890 1993;118(4):1095–106.
- 891 100. Gautam M, Noakes PG, Mudd J, Nichol M, Chu GC, Sanes JR, et al. Failure of postsynaptic specialization to develop at
892 neuromuscular junctions of rapsyn-deficient mice. *Nature.* 1995;377(6546):377232a0.
- 893 101. Dawson DM, Eppenberger HM, Eppenberger ME. Multiple Molecular Forms of Creatine Kinases. *Ann N Y Acad Sci.*
894 1968;151(1):616–26.
- 895 102. van Rooij E, Sutherland LB, Qi X, Richardson JA, Hill J, Olson EN. Control of {Stress-Dependent} Cardiac Growth and Gene
896 Expression by a {MicroRNA}. *Science (80-).* 2007;316(5824):575–9.
- 897 103. Hailstones D, Barton P, P C-T, Sasse S, Sutherland C, Hardeman E, et al. Differential regulation of the atrial isoforms of the myosin
898 light chains during striated muscle development. *J Biol Chem.* 1992;267(32):23295–300.
- 899 104. Marx SO, Reiken S, Hisamatsu Y, Jayaraman T, Burkhoff D, Rosembli N, et al. PKA Phosphorylation Dissociates FKBP12.6 from
900 the Calcium Release Channel (Ryanodine Receptor). *Cell.* 2004;101(4):365–76.
- 901 105. Kuro-o M, Nagai R, Tsuchimochi H, Katoh H, Yazaki Y, Ohkubo A, et al. Developmentally regulated expression of vascular smooth
902 muscle myosin heavy chain isoforms. *J Biol Chem.* 1989;264(31):18272–5.

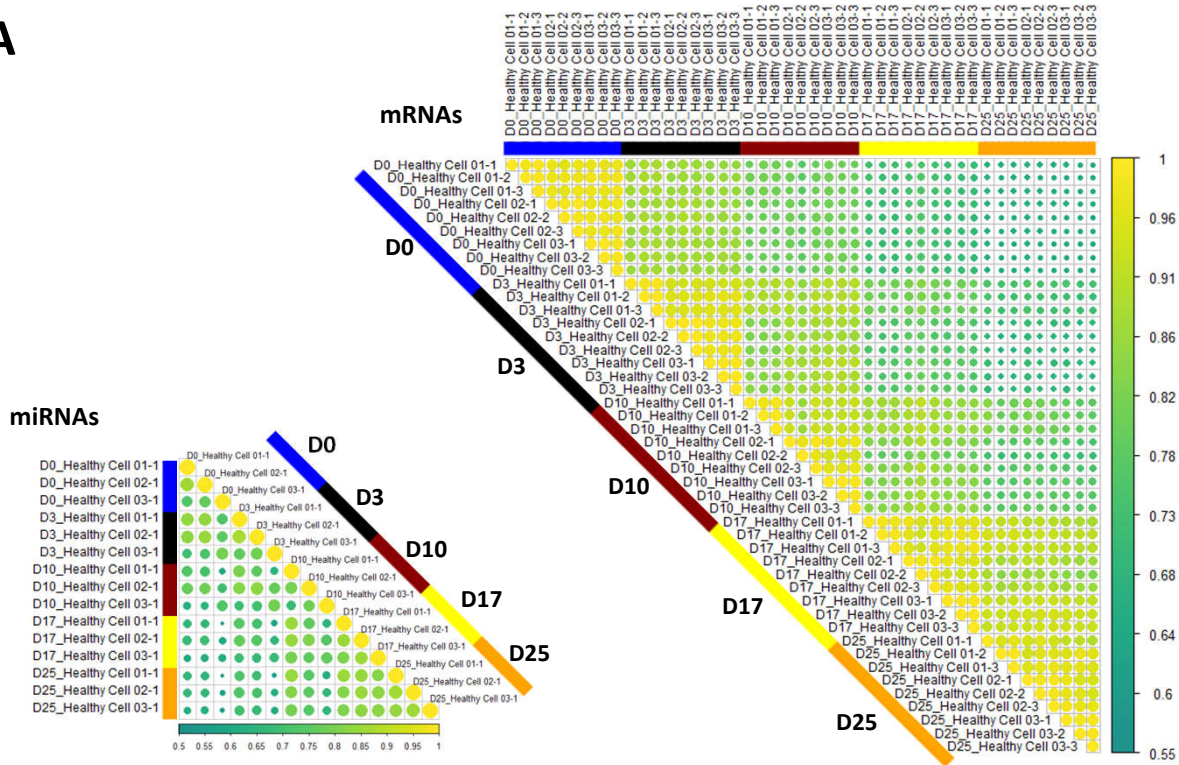
- 903 106. Gimona M, Herzog M, Vandekerckhove J, Small JV. Smooth muscle specific expression of calponin. *FEBS Lett.* 1990;274(1–
904 2):159–62.
- 905 107. Eglen RM, Reddy H, Watson N, Challiss RAJ. Muscarinic acetylcholine receptor subtypes in smooth muscle. *Trends Pharmacol Sci.*
906 1994;15(4):114–9.
- 907 108. Ajima R, Akazawa H, Kodama M, Takeshita F, Otsuka A, Kohno T, et al. Deficiency of Myo18B in mice results in embryonic
908 lethality with cardiac myofibrillar aberrations. *Genes to Cells.* 2008;13(10):987–99.
- 909 109. Heidmann O, Buonanno A, Geoffroy B, Robert B, Guenet JL, Merlie JP, et al. Chromosomal localization of muscle nicotinic
910 acetylcholine receptor genes in the mouse. *Science (80-).* 1986;234(4778):866–8.
- 911 110. Ueno T, Tanaka K, Kaneko K, Taga Y, Sata T, Irie S, et al. Enhancement of procollagen biosynthesis by p180 through augmented
912 ribosome association on the endoplasmic reticulum in response to stimulated secretion. *J Biol Chem.* 2010;285(39):29941–50.
- 913 111. Hautala T, Byers MG, Eddy RL, Shows TB, Kivirikko KI, Myllylä R. Cloning of human lysyl hydroxylase: Complete cDNA-derived
914 amino acid sequence and assignment of the gene (PLOD) to chromosome 1p36.3→p36.2. *Genomics.* 1992;13(1):62–9.
- 915 112. Valtavaara M, Papponen H, Pirttilä AM, Hiltunen K, Helander H, Myllylä R. Cloning and characterization of a novel human lysyl
916 hydroxylase isoform highly expressed in pancreas and muscle. *J Biol Chem.* 1997;272(11):6831–4.
- 917 113. Martens JHA, Verlaan M, Kalkhoven E, Zantema A. Cascade of Distinct Histone Modifications during Collagenase Gene Activation.
918 *Mol Cell Biol.* 2003;23(5):1808–16.
- 919 114. Long DA, Price KL, Ioffe E, Gannon CM, Gnudi L, White KE, et al. Angiotensin-1 therapy enhances fibrosis and inflammation
920 following folic acid-induced acute renal injury. *Kidney Int.* 2008;74(3):300–9.
- 921 115. Lipson KE, Wong C, Teng Y, Spong S. CTGF is a central mediator of tissue remodeling and fibrosis and its inhibition can reverse
922 the process of fibrosis. *Fibrogenesis Tissue Repair [Internet].* 2012;5(S1):S24. Available from:
923 <https://fibrogenesis.biomedcentral.com/articles/10.1186/1755-1536-5-S1-S24>
- 924 116. Fragiadaki M, Witherden AS, Kaneko T, Sonnylal S, Pusey CD, George B-G, et al. Interstitial fibrosis is associated with increased
925 {COL1A2} transcription in {AA-injured} renal tubular epithelial cells in vivo. *Matrix Biol.* 2011;30(7–8):396–403.
- 926 117. Hemmann S, Graf J, Roderfeld M, Roeb E. Expression of {MMPs} and {TIMPs} in liver fibrosis – a systematic review with special
927 emphasis on anti-fibrotic strategies. *J Hepatol.* 2007;46(5):955–75.
- 928 118. Duisters RF, Tijssen AJ, Schroen B, Leenders JJ, Lentink V, Van Der Made I, et al. MiR-133 and miR-30 Regulate connective tissue
929 growth factor: Implications for a role of micRNAs in myocardial matrix remodeling. *Circ Res.* 2009;104(2):170–8.
- 930 119. Vidal B, Serrano AL, Tjwa M, Suelves M, Ardite E, Mori R, et al. Fibrinogen drives dystrophic muscle fibrosis via a
931 {TGFβ/alternative} macrophage activation pathway. *Gene Dev.* 2008;22(13):1747–52.
- 932 120. Timpani CA, Hayes A, Rybalka E. Revisiting the dystrophin-ATP connection: How half a century of research still implicates
933 mitochondrial dysfunction in Duchenne Muscular Dystrophy aetiology. *Med Hypotheses.* 2015;85(6):1021–33.
- 934 121. Šileikyte J, Blachly-Dyson E, Sewell R, Carpi A, Menabò R, Di Lisa F, et al. Regulation of the mitochondrial permeability transition
935 pore by the outer membrane does not involve the peripheral benzodiazepine receptor (translocator protein of 18 kDa (TSPO)). *J*
936 *Biol Chem.* 2014;289(20):13769–81.
- 937 122. Emery AE, Burt D. Intracellular calcium and pathogenesis and antenatal diagnosis of Duchenne muscular dystrophy. *Br Med J.*
938 1980;280(6211):355–7.
- 939 123. Shkryl VM, Martins AS, Ullrich ND, Nowycky MC, Niggli E, Shirokova N. Reciprocal amplification of ROS and Ca²⁺ signals in
940 stressed mdx dystrophic skeletal muscle fibers. *Pflugers Arch Eur J Physiol.* 2009;458(5):915–28.
- 941 124. Whitehead NP, Yeung EW, Froehner SC, Allen DG. Skeletal muscle NADPH oxidase is increased and triggers stretch-induced
942 damage in the mdx mouse. *PLoS One.* 2010;5(12):e15354.
- 943 125. Rodriguez MC, Tarnopolsky MA. Patients with dystrophinopathy show evidence of increased oxidative stress. *Free Radic Biol*
944 *Med.* 2003;34(9):1217–20.
- 945 126. Scholte HR, Busch HFM. Early changes of muscle mitochondria in duchenne dystrophy Partition and activity of mitochondrial
946 enzymes in fractionated muscle of unaffected boys and adults and patients. *J Neurol Sci.* 1980;45(2–3):217–34.
- 947 127. Sharma U, Atri S, Sharma MC, Sarkar C, Jagannathan NR. Skeletal muscle metabolism in Duchenne muscular dystrophy {(DMD):}
948 an in-vitro proton {NMR} spectroscopy study. *Magn Reson Imaging.* 2003;21(2):145–53.
- 949 128. Lemos DR, Babaeijandaghi F, Low M, Chang C-K, Lee ST, Fiore D, et al. Nilotinib reduces muscle fibrosis in chronic muscle injury
950 by promoting {TNF-mediated} apoptosis of fibro/adipogenic progenitors. *Nat Med.* 2015;21(7):786–94.
- 951 129. Villalta AS, Nguyen HX, Deng B, Gotoh T, Tidball JG. Shifts in macrophage phenotypes and macrophage competition for arginine
952 metabolism affect the severity of muscle pathology in muscular dystrophy. *Hum Mol Genet.* 2009;18(3):482–96.
- 953 130. Desguerre I, Mayer M, Leturcq F, Barbet J-P, Gherardi RK, Christov C. Endomysial Fibrosis in Duchenne Muscular Dystrophy: A
954 Marker of Poor Outcome Associated With Macrophage Alternative Activation. *J Neuropathol Exp Neurol.* 2009;68(7):762–73.
- 955 131. Fusako S-T, Narita A, Masuda S, Wakamatsu T, Watanabe N, Nishiyama T, et al. Premyogenic progenitors derived from human
956 pluripotent stem cells expand in floating culture and differentiate into transplantable myogenic progenitors. *Sci Rep-uk.*
957 2018;8(1):6555.

- 958 132. Matsumura K, Tome FMS, Ionasescu V, Ervasti JM, Anderson RD, Romero NB, et al. Deficiency of dystrophin-associated proteins in Duchenne muscular dystrophy patients lacking COOH-terminal domains of dystrophin. *J Clin Invest.* 1993;92(2):866–71.
959
- 960 133. Yuasa K, Hagiwara Y, Ando M, Nakamura A, Takeda S, Hijikata T. {MicroRNA-206} is highly expressed in newly formed muscle
961 fibers: implications regarding potential for muscle regeneration and maturation in muscular dystrophy. *Cell Struct Funct.*
962 2008;33(2):163–9.
- 963 134. Cullen MJ, Fulthorpe JJ. Stages in fibre breakdown in duchenne muscular dystrophy An electron-microscopic study. *J Neurol Sci.*
964 1975;24(2):179–200.
- 965 135. Brouilly N, Lecroisey C, Martin E, Pierson L, Mariol MC, Mounier N, et al. Ultra-structural time-course study in the *C. elegans*
966 model for Duchenne muscular dystrophy highlights a crucial role for sarcomere-anchoring structures and sarcolemma integrity
967 in the earliest steps of the muscle degeneration process. *Hum Mol Genet.* 2015;24(22):6428–45.
- 968 136. Consolino CM, Brooks S V. Susceptibility to sarcomere injury induced by single stretches of maximally activated muscles of mdx
969 mice. *J Appl Physiol Bethesda Md* 1985. 2004;96(2):633–8.
- 970 137. Kong J, Anderson JE. Dystrophin is required for organizing large acetylcholine receptor aggregates. *Brain Res.* 1999;839(2):298–
971 304.
- 972 138. Kong J, Yang L, Li Q, Cao J, Yang J, Chen F, et al. The absence of dystrophin rather than muscle degeneration causes acetylcholine
973 receptor cluster defects in dystrophic muscle. *Neuroreport.* 2012;23(2):82–7.
- 974 139. Bell CD, Conen PE. Histopathological changes in Duchenne muscular dystrophy. *J Neurol Sci.* 1968;7(3):529–44.
- 975 140. Haddix SG, il Lee Y, Kornegay JN, Thompson WJ. Cycles of myofiber degeneration and regeneration lead to remodeling of the
976 neuromuscular junction in two mammalian models of Duchenne muscular dystrophy. *PLoS One.* 2018;13(10):e0205926.
- 977 141. Luz MAM, Marques MJ, Neto SH. Impaired regeneration of dystrophin-deficient muscle fibers is caused by exhaustion of
978 myogenic cells. *Braz J Med Biol Res.* 2002;35(6):691–5.
- 979 142. Zhou L, Porter JD, Cheng G, Gong B, Hatala DA, Merriam AP, et al. Temporal and spatial {mRNA} expression patterns of {TGF-
980 beta1,} 2, 3 and {TbetaRI,} {II,} {III} in skeletal muscles of mdx mice. *Neuromuscul Disord Nmd.* 2005;16(1):32–8.
- 981 143. Bernasconi P, Torchiana E, Confalonieri P, Brugnoli R, Barresi R, Mora M, et al. Expression of transforming growth factor-beta 1
982 in dystrophic patient muscles correlates with fibrosis. Pathogenetic role of a fibrogenic cytokine. *J Clin Invest.* 1995;96(2):1137–
983 44.
- 984 144. Takahashi K, Tanabe K, Ohnuki M, Narita M, Ichisaka T, Tomoda K, et al. Induction of Pluripotent Stem Cells from Adult Human
985 Fibroblasts by Defined Factors. *Cell.* 2007;131(5):861–72.
- 986 145. DREYFUS JC, SCHAPIRA G, SCHAPIRA F. Biochemical study of muscle in progressive muscular dystrophy. *J Clin Invest.*
987 1954;33(5):794–7.
- 988 146. Aschah A, Khairallah M, Daussin F, Bourcier-Lucas C, Godin R, Allen BG, et al. Stress-induced opening of the permeability transition
989 pore in the dystrophin-deficient heart is attenuated by acute treatment with sildenafil. *Am J Physiol Circ Physiol.*
990 2011;300(1):H144–53.
- 991 147. Pauly M, Daussin F, Burelle Y, Li T, Godin R, Fauconnier J, et al. AMPK activation stimulates autophagy and ameliorates muscular
992 dystrophy in the mdx mouse diaphragm. *Am J Pathol.* 2012;181(2):583–92.
- 993 148. M PC. {HISTOPATHOLOGICAL} {FEATURES} {OF} {MUSCLE} {IN} {THE} {PRECLINICAL} {STAGES} {OF} {MUSCULAR} {DYSTROPHY}.
994 *Brain.* 1962;85(1):109–20.
- 995 149. Bradley WG, Hudgson P, Larson PF, Papapetropoulos TA, Jenkinson M. Structural changes in the early stages of Duchenne
996 muscular dystrophy. *J Neurol Neurosurg Psychiatry.* 1972;35(4):451.
- 997 150. Rau F, Freyermuth F, Fugier C, Villemin JP, Fischer MC, Jost B, et al. Misregulation of miR-1 processing is associated with heart
998 defects in myotonic dystrophy. *Nat Struct Mol Biol.* 2011;18(7):840–5.
- 999 151. Singh A, Happel C, Manna SK, George A-M, Carrero J, Kumar S, et al. Transcription factor {NRF2} regulates {miR-1} and {miR-
1000 206} to drive tumorigenesis. *J Clin Invest.* 2013;123(7):2921–34.
- 1001 152. Zhang X, Zuo X, Yang B, Li Z, Xue Y, Zhou Y, et al. MicroRNA directly enhances mitochondrial translation during muscle
1002 differentiation. *Cell.* 2014;158(3):607–19.
- 1003 153. Fry CS, Kirby TJ, Kosmac K, McCarthy JJ, Peterson CA. Myogenic Progenitor Cells Control Extracellular Matrix Production by
1004 Fibroblasts during Skeletal Muscle Hypertrophy. *Cell Stem Cell.* 2017;20(1):56–69.
- 1005 154. Blau HM, Webster C, Pavlath GK. Defective myoblasts identified in Duchenne muscular dystrophy. *Proc Natl Acad Sci.*
1006 1983;80(15):4856–60.
- 1007 155. Bovolenta M, Erriquez D, Valli E, Brioschi S, Scotton C, Neri M, et al. The DMD Locus Harbours Multiple Long Non-Coding RNAs
1008 Which Orchestrate and Control Transcription of Muscle Dystrophin mRNA Isoforms. *PLoS One.* 2012;7(9).
- 1009 156. Ervasti JM, Campbell KP. A role for the dystrophin-glycoprotein complex as a transmembrane linker between laminin and actin. *J*
1010 *Cell Biol.* 1993;122(4):809–23.
- 1011 157. Muntoni F, Melis MA, Ganau A, Dubowitz V. Transcription of the dystrophin gene in normal tissues and in skeletal muscle of a
1012 family with X-linked dilated cardiomyopathy. *Am J Hum Genet.* 1995;56(1):151–7.

- 1013 158. Warner LE. Expression of Dp260 in muscle tethers the actin cytoskeleton to the dystrophin-glycoprotein complex and partially
1014 prevents dystrophy. *Hum Mol Genet.* 2002;11(9):1095–105.
- 1015 159. Dooreenweerd N, Mahfouz A, Van Putten M, Kaliyaperumal R, T’Hoen PAC, Hendriksen JGM, et al. Timing and localization of
1016 human dystrophin isoform expression provide insights into the cognitive phenotype of Duchenne muscular dystrophy. *Sci Rep.*
1017 2017;7(1).
- 1018 160. Lu-Nguyen N, Ferry A, Schnell FJ, Hanson GJ, Popplewell L, Dickson G, et al. Functional muscle recovery following dystrophin and
1019 myostatin exon splice modulation in aged mdx mice. *Hum Mol Genet.* 2019;
- 1020 161. Peccate C, Mollard A, Le Hir M, Julien L, McClorey G, Jarmin S, et al. Antisense pre-treatment increases gene therapy efficacy in
1021 dystrophic muscles. *Hum Mol Genet.* 2016;25(16):3555–63.
- 1022 162. Morales MG, Gutierrez J, Cabello-Verrugio C, Cabrera D, Lipson KE, Goldschmeding R, et al. Reducing CTGF/CCN2 slows down
1023 mdx muscle dystrophy and improves cell therapy. *Hum Mol Genet.* 2013;22(24):4938–51.
- 1024 163. Gatliff J, Campanella M. {TSP0:} kaleidoscopic {18-kDa} amid biochemical pharmacology, control and targeting of mitochondria.
1025 *Biochem J.* 2016;473(2):107–21.
- 1026 164. Massouridès E, Polentes J, Mangeot P-EP-E, Mournetas V, Nectoux J, Deburgrave N, et al. Dp412e: a novel human embryonic
1027 dystrophin isoform induced by BMP4 in early differentiated cells. *Skelet Muscle* [Internet]. 2015 Dec 14 [cited 2017 Feb
1028 27];5(1):40. Available from: <http://www.skeletalmusclejournal.com/content/5/1/40>
- 1029 165. Köster J, Rahmann S. Snakemake—a scalable bioinformatics workflow engine. *Bioinformatics.* 2012;28(19):2520–2.
- 1030 166. Dobin A, Davis C a, Schlesinger F, Drenkow J, Zaleski C, Jha S, et al. STAR: ultrafast universal RNA-seq aligner. *Bioinformatics*
1031 [Internet]. 2013 Jan 1 [cited 2014 Jul 13];29(1):15–21. Available from:
1032 <http://www.pubmedcentral.nih.gov/articlerender.fcgi?artid=3530905&tool=pmcentrez&rendertype=abstract>
- 1033 167. Wang L, Wang S, Li W. RSeQC: quality control of RNA-seq experiments. *Bioinformatics* [Internet]. 2012 Aug 15 [cited 2017 Jul
1034 6];28(16):2184–5. Available from: <https://academic.oup.com/bioinformatics/article-lookup/doi/10.1093/bioinformatics/bts356>
- 1035 168. Liao Y, Smyth GK, Shi W. FeatureCounts: An efficient general purpose program for assigning sequence reads to genomic features.
1036 *Bioinformatics* [Internet]. 2014 Apr 1 [cited 2017 Jul 6];30(7):923–30. Available from:
1037 <http://www.ncbi.nlm.nih.gov/pubmed/24227677>
- 1038 169. Ewels P, Magnusson M, Lundin S, Källér M. MultiQC: Summarize analysis results for multiple tools and samples in a single report.
1039 *Bioinformatics* [Internet]. 2016 Oct 1 [cited 2017 Jul 6];32(19):3047–8. Available from:
1040 <https://academic.oup.com/bioinformatics/article-lookup/doi/10.1093/bioinformatics/btw354>
- 1041 170. Love MI, Huber W, Anders S. Moderated estimation of fold change and dispersion for RNA-seq data with DESeq2. *Genome Biol*
1042 [Internet]. 2014;15(12):550. Available from: <http://genomebiology.biomedcentral.com/articles/10.1186/s13059-014-0550-8>
- 1043 171. Durinck S, Spellman PT, Birney E, Huber W. Mapping identifiers for the integration of genomic datasets with the R/ Bioconductor
1044 package biomaRt. *Nat Protoc* [Internet]. 2009 [cited 2019 Jun 12];4(8):1184–91. Available from:
1045 <http://www.ncbi.nlm.nih.gov/pubmed/19617889>
- 1046 172. Schmieder R, Edwards R. Quality control and preprocessing of metagenomic datasets. *Bioinformatics.* 2011;27(6):863–4.
- 1047 173. Martin M. Cutadapt removes adapter sequences from high-throughput sequencing reads. *Embnet J.* 2011;17(1):10–2.
- 1048 174. Amrhein V, Greenland S, Blake M. Scientists rise up against statistical significance. *Nature.* 2019;567(7748):305–7.
- 1049 175. Garnier S. viridis: Default Color Maps from “matplotlib”. R package version 0.5.1. 2018; Available from: <https://cran.r-project.org/package=viridis>
- 1051 176. Simko TW and V. R package “corrplot”: Visualization of a Correlation Matrix (Version 0.84). 2017; Available from:
1052 <https://github.com/taiyun/corrplot>
- 1053 177. Gregory R, Warnes, Ben Bolker, Lodewijk Bonebakker, Robert Gentleman, Wolfgang Huber Andy Liaw, Thomas Lumley M,
1054 Maechler, Arni Magnusson, Steffen Moeller MS and BV. gplots: Various R Programming Tools for Plotting Data. R package
1055 version 3.0.1. 2016; Available from: <https://cran.r-project.org/package=gplots>
- 1056 178. Fresno C, Fernández EA. {RDAVIDWebService:} a versatile R interface to {DAVID}. *Bioinformatics.* 2013;29(21):2810–1.
- 1057

Figure 1

A



B

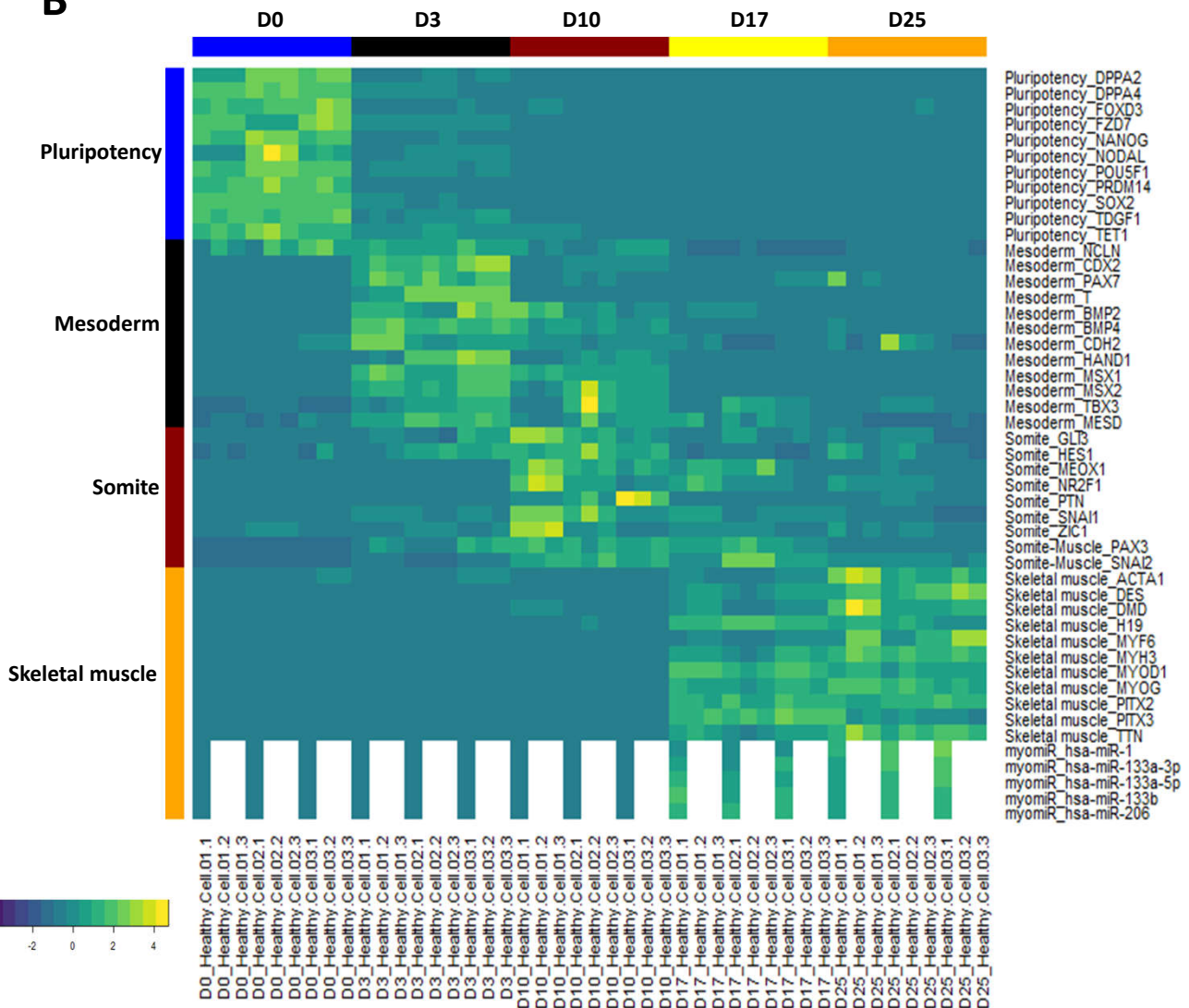


Figure 2

